8-2021

An Electrochemical Immunoassay System for Measuring Circulating Protein Biomarkers of Pediatric Soft Tissue Sarcoma

Ivy Antwi
East Tennessee State University

An Electrochemical Immunoassay System for Measuring Circulating Protein Biomarkers of

Pediatric Soft Tissue Sarcoma

_____

A thesis

presented to

the faculty of the Department of Chemistry

East Tennessee State University

In partial fulfillment

of the requirements for the degree

Master of Science in Chemistry

_____

by

Ivy Antwi

August 2021

_____

Gregory W. Bishop, Ph.D., Chair

Catherine E. McCusker, Ph.D.

Dane W. Scott, Ph.D.

Keywords: biomarkers, 3D-printing, electrochemical immunoassay, biosensors, pediatric cancer

ABSTRACT

An Electrochemical Immunoassay System for Measuring Circulating Protein Biomarkers of

Pediatric Soft Tissue Sarcoma

by

Ivy Antwi

Measurement of circulating protein biomarkers associated with disease can facilitate early

detection, help guide treatment strategies and improve patient outcomes beyond current standards

of care. The combination of inexpensive 3D-printed flow cells and electrochemical biosensors has

recently emerged as a viable platform for low-cost, reliable biomarker measurements. Here, we

report an electrochemical immunoassay system based on simple graphite electrode arrays, 3D-

printed flow cells, and signal-generating magnetic bead bioconjugates for simultaneous detection

of three biomarker proteins (cancer antigen 125 (CA 125), midkine (MK) and osteopontin (OPN))

associated with pediatric soft tissue sarcomas. Magnetic bead bioconjugates are functionalized

with large amounts of antibody and enzyme labels, electrode arrays are modified with gold

nanoparticles and antibodies for specific capture of bioconjugate-labeled biomarkers, and 3D-

printed flow cells facilitate their amperometric detection. Using this system, detection limits for

CA 125, OPN and MK are 100 times lower than those obtained with commercial enzyme-linked

immunosorbent assay.

DEDICATION

This thesis is dedicated to my family and friends for their immense contribution to the success of this program.

ACKNOWLEDGMENTS

TABLE OF CONTENTS

LIST OF TABLES

LIST OF FIGURES

LIST OF ABBREVIATIONS

4-PL: 4-parameter log

Ab1: Capture antibody

Ab2: Detection antibody

ABTS: 2,2'-azino-bis (3-ethylbenzothiazoline-6-sulfonic acid)

ALP: Alkaline Phosphatase

ASTM: American society for testing and materials

BSA: Bovine serum albumin

CA 125: Cancer antigen 125

CAD: Computer-aided design

CV: Cyclic voltammetry

DLP: Digital light processing

EDC: 1-ethyl-3-(3-dimethyl aminopropyl) carbodiimide

ELISA: Enzyme-linked immunosorbent assay

FDM: Fused deposition modeling

GSH-AuNPs: Glutathione-capped gold nanoparticles

HRP: Horseradish peroxidase

LbL: Layer-by-layer

LC-MS: Liquid chromatography-mass spectrometry

MB: Magnetic beads

MK: Midkine

NHS: N-hydroxysuccinimide

NSB: Nonspecific binding

OPN: Osteopontin

PBS: Phosphate buffered saline

PDDA: Poly (diallyl dimethylammonium chloride)

POCT: Point-of-care testing

PS-NCAM: Polysialylated neural cell adhesion molecule

PSTS: Pediatric soft tissue sarcoma

SIMOA: Single molecule array

SLA: Stereolithography

SLS: Sodium lauryl sulfate

SPR: Surface plasmon resonance

CHAPTER 1. INTRODUCTION

Biomarkers and Disease

Biomarkers have been defined broadly by the World Health Organization as 'any measurable process, substance, structure or products of reactions in the body that can predict or influence the incidence of outcome or disease'.[1,2] Measurements of biomarker levels can be used to determine a person's health status or predict the outcome of a disease.[3] For example, heart rate on an electrocardiogram serves as a biomarker to check damage to the heart, and blood glucose level is a biomarker for diabetic ketoacidosis.[4] The quality of biomarkers can be characterized in terms of parameters known as sensitivity and selectivity. Ideal biomarkers exhibit high specificity (low false positive rate) and sensitivity (low false negative rate).[5]

Since some circulating proteins are over- or under-expressed in the body due to certain diseases or health conditions, proteins are an important class of biomarkers. One example of a protein biomarker is C-reactive protein, which gives information about the rate of inflammation in colons of cancer patients.[6] For effective indication of the current medical state of a person, protein biomarkers must be measured accurately and reproducibly in serum, blood, urine, or soft tissue samples. The most widely used technique in clinical analysis of protein biomarkers continues to be traditional enzyme-linked immunosorbent assay (ELISA).[7]

Enzyme-linked Immunosorbent Assay

ELISA is based on the specific binding interaction between an antibody and the biomarker of interest (antigen), and an optical signal (e.g., optical density or absorbance) generated by an enzyme reaction (Figure 1). There are a few different forms on ELISA such as direct, indirect, competitive and sandwich ELISA.[8] However, the most common is the sandwich-type due to its high sensitivity.[8]
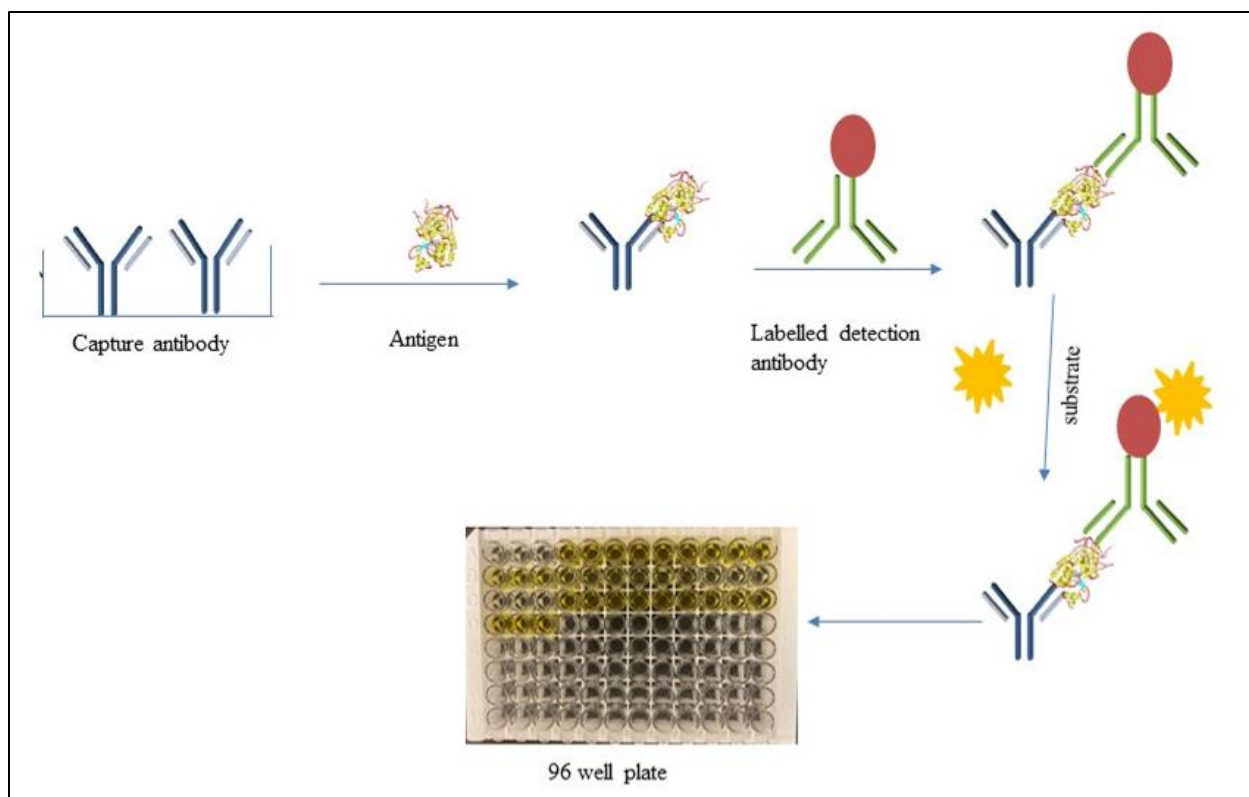
Figure 1. An illustrated schematic diagram for sandwich-type immunoassay

In sandwich-type ELISA, a primary antibody that has high specificity for the antigen is bound onto a surface such as the wells in a microtiter plate. The sample (e.g., serum) is delivered into the well so that the antigen can be captured by the primary antibody and thus isolated from the rest of the sample matrix. Following washing steps to remove unbound or weakly bound materials, a second antibody, labeled with an enzyme, is introduced into the wells where it binds to the captured analyte, forming a sandwich-like bioconjugate. Detection of analyte is achieved by adding an enzyme substrate which strongly absorbs visible light upon reaction with the enzyme.[7] The most commonly used enzymes in ELISA are horseradish peroxidase (HRP) and alkaline phosphatase (ALP) which are activated by hydrogen peroxide and p-nitrophenyl-phosphate, respectively. In the case of HRP, the addition of hydrogen peroxide oxidizes Fe(III)

center which generates an optical signal in the form of a color change upon the addition of a substrate like 2,2'-azino-bis(3-ethylbenzothiazoline-6-sulfonic acid (ABTS).[8-11]

ELISAs are very useful techniques in quantifying protein biomarkers in serum and other biological fluids. Typical ELISA techniques exhibit detection limits ranging from 1-100 pg/ml (picogram per milliliters) which are insufficient for detection of protein biomarkers of cancer at early stages.[12] They also pose great challenges due to other limitations, such as long analysis time and relatively large sample volume requirements (typically 100 µl). ELISA techniques are also typically confined to centralized lab settings with requisite instrumentation and expertise, and they are poorly suited for measurements of more than a single protein biomarker in a given aliquot of sample.[13]

While interest in identifying and studying biomarkers has been well-established for decades, contemporary advances in research and technology have enabled more convenient and effective capture, isolation, detection, and characterization of biomarker proteins in clinical samples.[14] These advances and continuing accumulation of knowledge of the relationship between diseases and circulating proteins, has also led to a strong emphasis on the development of biomarker panels (i.e., collections of proteins). The interest in biomarker panels stems from the highly complex and diverse nature of diseases such as cancers, which often renders single protein measurements insufficient in terms selectivity and specificity for a particular disease.[15]

A few commercialized techniques are suitable for measuring protein biomarker panels. Modern liquid chromatography-mass spectrometry (LC-MS) proteomics has been able achieve multiple protein biomarker measurements in clinical samples. LC-MS proteomics also typically has acceptable sensitivity and a lower limit of detection as compared to traditional ELISA.

However, it is very expensive and also involves quite complex instrumentation and techniques and, as such, very difficult to be used outside of clinical settings.[7,12]

Another technique with high sensitivity and selectivity that can be employed in biomarker detection is the single molecule array (Simoa™), which has recently been commercialized by David Walt.[16] This system is similar to conventional ELISA. However, in place of a single antibody labeled with a single enzyme, an enzyme-labeled immunocomplex is formed on a paramagnetic bead (MB) that features many copies of a specific antibody. The MB immunocomplex is subsequently isolated in a single well of femtoliter volume prepared from an array of etched optical fibers. The diameter of each well is such that only a single MB immunocomplex can fit.[17] This system requires proprietary reagents, sophisticated instrumentation, and a centralized lab for sample processing.

Thus, inexpensive, simple, easy to operate and reliable sensing systems and strategies for measuring multiple protein biomarkers remains a largely unmet challenge that is the subject of continuing research and development. Strategies for analyzing clinical samples for multiple protein biomarkers based on electrochemical measurements (e.g., electrochemical immunoassays) have gained great attention due to low cost, lack of maintenance and relative ease of miniaturization associated with electrochemical instruments, and relative ease at which sensitive analytes can be measured electrochemically in low sample volumes.[18,19]

Electrochemical Immunoassay and Immunosensors

Electrochemical immunoassays were first reported by Heineman et al. in 1979.[20,21] In electrochemical immunoassays, an amperometric, conductometric, or potentiometric signal is generated as the bioreceptor (antibody) interacts with the antigen, and the electrochemical signal is used to determine the antigen (target analyte) concentration.[10,11,19,22] While there are several

15

different forms of electrochemical immunoassays, many are based on the sandwich-type strategy (Figure 2) where an antibody (biorecognition molecule) is immobilized on an electrode surface to specifically bind an antigen (target analyte) and the electrochemical signal is generated by a label (e.g., enzyme, metal nanoparticle, redox species) that is attached to another antibody which also binds to the antigen.[23] Strategies where an enzyme label is used to generate the electrochemical signal are forms of ELISA with electrochemical detection (i.e., electrochemical ELISA).[24]
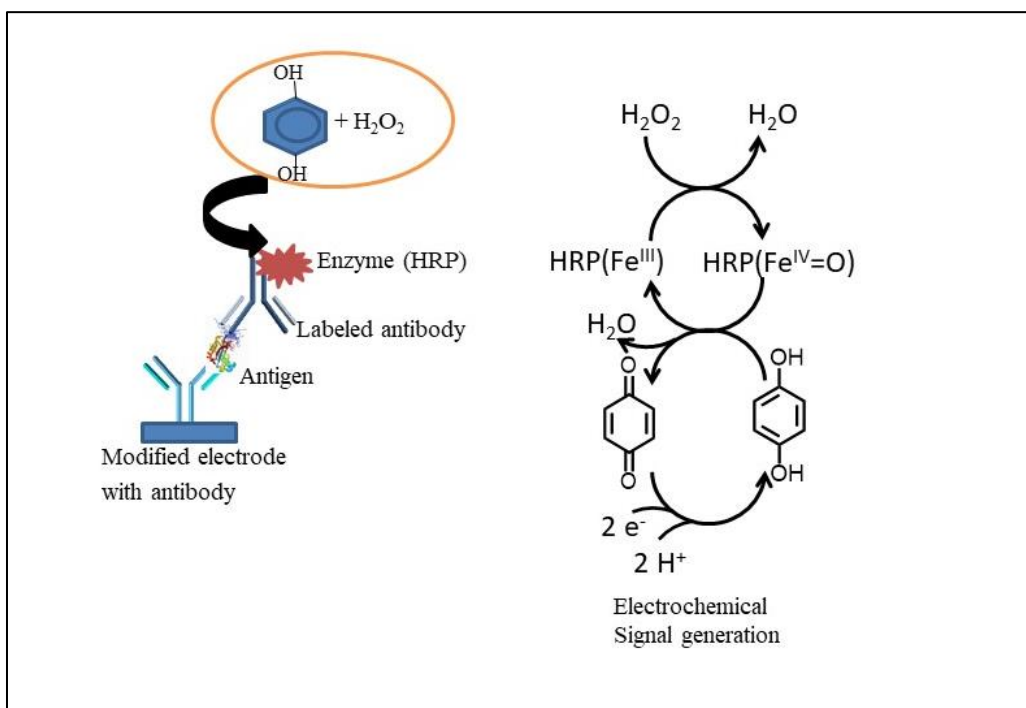
Figure 2. Illustration of an electrochemical sandwich-type ELISA

Many electrochemical immunoassay strategies have since been developed and reported to increase sensitivity (Table 1). One way of enhancing signal is by increasing the number of signal-generating labels on the detection antibodies, which can be done by providing support such as polymers or magnetic microbeads.[3]

Table 1. List Of Some Antigen, Labels and Electrodes Used in Electrochemical Immunoassays with its Limit of Detection

Target Antigen	Label	Electrode	LOD	Linear Range	Ref
(IL)-8 mRNA &	Antifluorescein-HRP	Streptavidin-coated Au electrode	3.9 fM	5fM - 50pM	25
(IL)-8	HRP-Ab$_2$		7.4 pg/ml	10 - 500 pg/ml	
PSA	Ab2-MB-HRP	AuNP Pyrolytic graphite electrode	0.5 pg/ml	0 -10 pg/ml	81
IL-6	MWCNT-HRP-Ab$_2$	SWNT forest electrode	0.5 pg/ml	0.5 - 5pg/ml	26
f-PSA	Ab$_2$-HRP	MB - SPCE	< 0.1 ng/ml	0 - 1 ng/ml	27
PSA	Ab$_2$ -AP	SPCE	1.4 ng/ml	0 – 20 ng/ml	28
CEA	MB-Au-HRP	AuNP-CFME	10 pg/ml	0.01 -160 ng/ml	29
AFP	No label	MWCNT-Ag glassy carbon electrode	8 pg/ml	0.25 – 250 ng/ml	30
Cardiactroponin1	Au	MCM-MCPE	0.5 ng/ml	0.8 – 5 ng/ml	31
PSA & IL-6	MB-HRP-Ab$_2$	AuNP -SPCE	0.23 pg/ml 0.30 pg/ml	0.225 – 5 pg/ml 0.30 – 20 pg/ml	32
PSA, VEGF-D, ERG & IGF-1	Poly-HRP-Ab$_2$	AuNP-SPCE	0.22 ± 0.05 zmol 0.341 ± 0.036 zmol 0.034 ± 0.002 zmol 0.083 ± 0.0012 zmol	0.06 -1044 fg/ml 0.04 – 7726 fg/ml 0.02 -149 fg/ml 0.01 – 52 fg/ml	37

The Rusling group has developed an ultrasensitive electrochemical immunoassay strategies based on magnetic microbeads modified with large numbers of antibodies (~90,000) and enzyme labels (~200,000) for multiplexed measurements of biomarker proteins.[3,26,32,34-36]

The strategy also involves nanomaterial-modified or nanostructured electrode arrays housed in simple fluidic devices to enable sandwich-type electrochemical ELISA with flow-through amperometric detection. Electrode arrays are made by modifying the surfaces of electrodes (e.g., screen-printed carbon, gold film, etc.) with metal nanoparticles (AuNP) or carbon-based nanomaterials to enhance electrochemical signal and antibodies for capture of antigens that are labeled with magnetic bead bioconjugates (Table 1).

During immunoassays, electrode arrays are housed in simple polydimethylsiloxane (PDMS)-based fluidic devices (volume <~100 μL), which are prepared from machined molds. A simple syringe pump and manual injector are used to deliver reagents, washing solutions, and magnetic bead bioconjugate labels to the electrode array. Due to the large numbers of antibodies and enzymes on the magnetic beads along with the nanostructured electrode array surfaces, detection limits for various proteins related to prostate and oral cancers have been reported in the low fg/mL (femtogram per milliliters) range with this strategy. This is ~100-1000 times better than traditional ELISA methods.[32-36] For example, using this system, Chikkaveeraiah et al. reported a multiplex detection of two biomarker proteins, prostate-specific antigen (PSA) and interleukin-6 (IL-6) at a sub pg/ml level. Detection limits of 0.30 pg/ml and 0.23 pg/ml for IL-6 and PSA, respectively, were achieved with magnetic particles heavily conjugated with detection antibodies (~9.0 x 10^4 active antibody) and enzyme labels (HRP) (~2.0 x 10^5 active HRP). This report showed a great correlation with ELISA and an improvement on it given how the system measured lower concentration at an analysis time of 1.15h (Table 1).[32]

In another study from Rusling's group, Dhanapala et al. reported multiplex detection of four biomarkers using a similar strategy. However, in place of magnetic beads, a commercially available polymer modified with a large number of HRP enzymes was used to increase

18

sensitivity. They reported, an unmatched sensitivity of sub-zeptomole and ultra-low detection limit 0.08-0.22 zmol (zeptomole) when vascular endothelial growth factor -D (VEGF-D), prostate-specific antigen (PSA), insulin-like growth factor-1 (IGF-1), and EST-related gene protein (ERG) were measured in post-prostatectomy patient serum having low levels of analytes (Table 1).[37]

Although Rusling's group used simple PDMS-based microfluidic devices for compatibility with low sample volumes (≤100 µl), the modular design of the system (i.e., two-sided PDMS channel with top and bottom sides defined by hard acrylic plates secured together with screws) requires manual positioning of electrodes, assembly and disassembly to complete each assay.[38] The dimensions of the PDMS channels are also typically too large (i.e., 1.5 mm wide, 2.8 cm long) to fit most common definitions of microfluidics. As an alternative for simple fabrication of microfluidic devices, Bishop et al. and others have recently explored the use of 3D printing in making fluidic channels.[39-47]

3D-Printed Fluidic Devices

3D printing, also known as additive manufacturing, generally involves deposition, curing or sintering of materials in successive layers to create a three-dimensional object from a model, which can be prepared with the help of computer-aided design (CAD) software.[48] Materials such as ceramics, thermoplastics, metals, and graphene-based materials are some examples of materials 3D printing technologies can print and can be in either liquid or powder form.[38] In recent years, 3D printing has found widespread use in research, aerospace, biomedical, art and design, defense, etc.[49]

While the first 3D printing technology, referred to as stereolithography (SLA), was commercialized by Charles Hull in the late 1980s, it has evolved especially rapidly over the past

decade and a half.[50] There are currently at least eighteen 3D printing methods that employ a host

of diverse printing materials.[43] These have been cataloged into seven groups according to

Standard F2792 of the American Society for Testing and Materials (ASTMs).[51] SLA and fused

deposition modeling (FDM) are some examples of available printing technologies with the most

cost-effective desktop printers with a price range of less than one hundred to a few thousand

dollars.[38] In SLA, a light source (e.g., a laser or projector lamp) cures a photosensitive resin,

while FDM employs a heated nozzle to extrude and deposit thermoplastic filament.

While fluidic devices have been prepared with several 3D printing techniques, including SLA,

FDM, and polyjet (i.e., photocuring of jettable inks) technologies, SLA continues to be one of

the most promising techniques in printing truly microfluidic channels due to its relatively high

resolution[43] and low cost compared to other methods.[39]

Stereolithography Printing Technique

SLA printers rely on vat photopolymerization mechanism for printing.[49] In this

technique, a photosensitive resin is polymerized by a light source (e.g., laser, or light-emitting

diode or mercury vapor lamp in a projector). The system consists of a vat, or container for

photosensitive resins, a platform for deposition of cured resin layers, a positioning system for

moving the platform and vat between curing cycles, and a light source for curing the resin. The

resins used in SLA generally consist of (acrylate or epoxy) monomers, a photoinitiator (e.g.,

phenylbis(2,4,6-trimethylbenzoyl)phosphine oxide), and an absorbing species (e.g., Sudan I) that

is used to regulate the incident light penetration depth.[39] While some systems (including Hull's

original design) employ lasers for curing, digital light processing (DLP) projectors equipped with

light emitting diodes have become much more common sources in recent years as such

projectors can cure each layer by a single exposure (Figure 3).

20
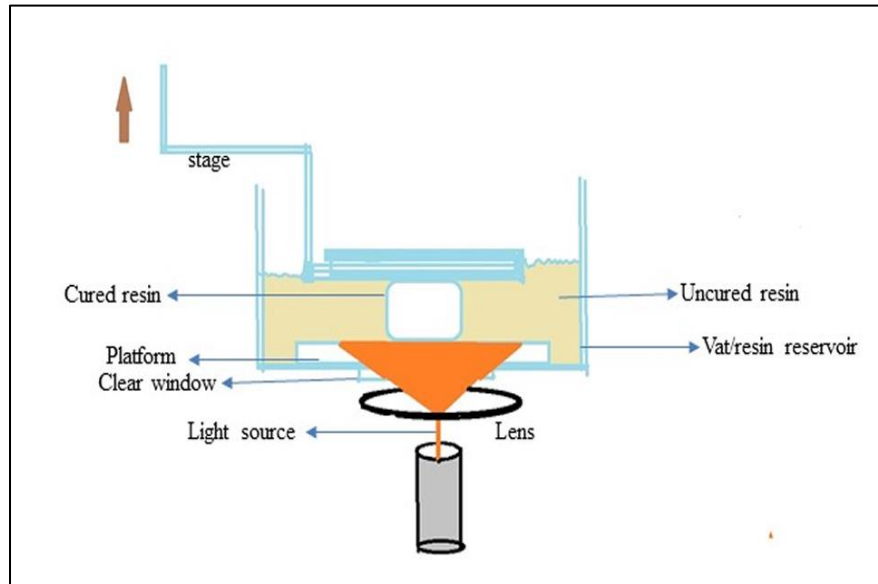
Figure 3. Schematic representation of DLP based SLA technique

3D Printed Microfluidic Devices

Many researchers, including Bharhava et al.,[52] Shallan et al.,[53] and Fang et al.,[54] have successfully printed fluidic devices using low-cost commercially available resins and SLA-type printers. However, fluidic devices prepared using SLA often have channels with cross-sectional dimensions of 200 µm to 1000 µm, which are often considered too large for microfluidics and have been instead deemed millifluidics. In this traditional SLA, printing resolution is based on the laser spot size or pixel size of projected light source. It is often difficult to make truly microfluidic devices using SLA due to overcuring of the resin that resides in the fluidic channel during printing, which results in blockage of small channels.[55]

Recently Nordin's group has demonstrated the combination of SLA-DLP printing technique with custom-formulated resins can enable 3D printing of microfluidic devices with high resolution (27 µm in X-Y plane, 1 mm increment in the Z axis). In one report, they demonstrated that controlling the concentration of absorbing species and photoinitiator in

21

formulated resins limits light penetration during exposure which then makes it possible for the

source spectrum to be fully covered by the absorber's spectrum and limits overcuring of resin in

small channels. Using these strategies, they have reported microfluidic channels with cross

sectional dimensions as low as 18 µm x 20 µm.[39,41,42] While 3D printing of microfluidic devices

is not yet routine, SLA remains a promising candidate with proven capabilities in this regard.[56]

3D Printed Fluidic Device with Electrochemical Sensors

Over the years, the combination of electrochemical immunoassays with 3D-printed

fluidic devices has been of particular interest to researchers due to its potential for automation

and miniaturization for point-of-care and clinical use.[21,22] Along these lines, researches have

explored several strategies for interfacing electrodes with 3D-printed fluidic devices.[57]

One recently reported strategy is the fully embedding electrodes into 3D printed devices.

For example, Castiaux et al.[58], reported the use of polyjet printing to directly embed a platinum

black electrode and counter electrode into a fluidic device for the electrochemical detection of

nitric oxide. This printing process used a stacked printing technique. Separate layers of the

device is printed and depending on where electrodes will be embedded, the layers are stacked

together into a single device with electrodes embedded using epoxy. Although this approach of

directly embedding electrodes during printing process brings about a robust sense of ease and

transferability for electrochemical sensing, electrodes fabricated this way are not reusable and

polyjet printing technique is costly.

Another strategy that is gaining popularity is the use of FDM printers to fully print fluidic

devices that feature incorporated sample processing and sensing elements, including electrodes,

valves, and pumps, in one step.[59] O'Neil et al.[60] demonstrated the use of FDM printing technique

to successful print a single step electrochemical flow-cell which simultaneously incorporated

graphene composite poly(lactic acid) electrode and poly (lactic acid) insulator during the printing process. Although this approach is promising, FDM lacks resolution to prepare microfluidic channels. Devices printed with these strategies often cannot be reused, and applications may be limited due to challenges associated with modifying electrodes directly printed in the fluidic device.

Another approach reported for 3D-printed electrochemical sensors is the modular incorporation of reusable electrodes into 3D-printed fluidic devices. In this approach, openings or ports are designed in the fluidic device so that electrodes, housed in commercially available or 3D-printed fittings, can be inserted into and removed from the fluidic channel as desired. With this approach, electrodes can be polished and subsequently reused for electrochemical detection after exposure to other analytes.[46,47]

Using this modular electrode incorporation strategy together with biosensing strategy previously reported by Jim Rusling's group, Abdulhamid reported successful detection of S100B, a protein biomarker associated with skin cancer and brain injury.[7] In his report, a low-cost graphite electrode modified with glutathione-capped gold nanoparticles was integrated into an SLA-prepared 3D printed fluidic device (800 µm by 800 µm cross-section). The fluidic device featured outlet and inlet threaded ports that allowed the injection of reagents in and out of the channel and a central threaded port where the modified electrode for the electrochemical sensing was integrated.

Research Aims

Current clinical measurement of biomarkers proteins requires considerable time and cost. However, recent research has shown that these measurements can be done via a combination of the low-cost 3D printed flow cell and low-maintenance electrochemical biosensors. To date, this

promising way of analyzing protein biomarkers has only been applied to protein biomarkers associated with oral and prostate cancer.[61,62] As a result, the main goal of this research is to apply this strategy to develop a highly reliable biosensing system, that would be capable of measuring multiple circulating biomarkers associated with Pediatric Soft Tissue Sarcoma (PSTS).

PSTS are fast-growing, uncontrollable tumors, which make up about 7% of all infancy tumors and is the sixth most common cancer disease in children.[63] These are classified into the rhabdomyosarcomas (RMS), which account for 4% of infancy tumors, and the non-rhabdomyosarcomas (nRMS) soft tissue sarcomas, which also constitute about another 3%. Although PSTS account for 7% of childhood cancer, the overall 5-year survival rate is fairly poor (10% to 30%)[64] in patients with the metastatic diseases. Surgery is the most common treatment method for soft tissue sarcomas at the early stage, and for the last or extreme tumor stage radiation being employed. About 40% to 50% of children with soft tissue sarcoma experience the re-occurrence of the disease, which is almost always deadly, despite good local control.[63] There has been no standard staging system reported for PSTS.

Due to the increasing number of molecular genetic alterations occurring in the tumor (sarcomas), soft tissue tumors are also categorized into two groups. One exhibits genetic modifications. Another one exhibits several compounded karyotypic abnormalities with no form. Some serum biomarkers for sarcomas are recently reported, including creatine kinase MB, cancer antigen 125 (CA 125), polysialylated neural cell adhesion molecule (PS-NCAM), midkine (MK), and osteopontin (OPN).[65]

In a study conducted by Lucas et al., midkine levels in sera sample of patients with embryonal pediatric tumors were compared to a vast number of children without the disease. The

study was conducted in 215 children without the disease and 29 pediatric patients with embryonal tumors consisting of rhabdomyosarcomas (5), nephroblastoma (14), and neuroblastoma (10) using an ELISA test. They reported a significantly higher MK levels in tumor patients, recording a mean concentration of 0.62 ng/ml than in patients without the disease recording a median concentration of 0 ng/ml (0 ng/ml at 25th percentile and 0.31 ng/ml at 75th percentile). From their research findings, patients with rhabdomyosarcoma showed elevated MK concentration in the collected sera sample with concentration as high as 52 ng/ml (median 0.29 ng/ml).[66]

Bache et al. conducted a study to ascertain association of OPN levels with patients with soft tissue sarcoma. In this study, serum sample of 93 soft tissue sarcoma patients were analyzed with an ELISA assay. They confirmed the presence of OPN in these serum samples with a median concentration of 704 ng/ml (184-2660 ng/ml). They also confirmed the OPN levels in serum was associated with clinical parameters such as tumor size, tumor grade etc.[67] The efficient clinical applications of these serum biomarkers have not been reported yet. As more advanced attempts are needed to prove the clinical role of serologic tests in this malignancy, the recognition of distinctive serum signatures for PSTS may lay out important value to detection, precise prognosis and assessment of disease or ailment, and progress of treatment.[32]

In working towards achieving this goal, low-cost graphite electrode arrays were modified with commercially available antibodies of MK, OPN, and CA 125 and subsequently integrated into 3D- printed flow cells developed in-house using a desktop 3D printer through previously reported strategies by Bishop et al.[40] and Adulhamid.[7] The sandwich electrochemical immunoassay was developed using previously reported strategies and experiences from

Rusling's group.[3,13,32,34-36] With this new measurement system developed, it will enable the

analysis of human serum samples obtained from PSTS patients and controls via biorespository.

CHAPTER 2. EXPERIMENTAL

Chemicals and Instrumentation

Duosets containing antigen, capture and biotinylated detection antibodies of protein CA 125, OPN, and MK as well as streptavidin-HRP and enzyme substrate for ELISA development were obtained from R&D Systems. The duoset antibodies and antigens were also used for development of electrochemical ELISA. ProMag 1 magnetic microbeads (mean diameter: 0.80 µm, density: $1.8g/cm^3$) were supplied by Bangs Laboratories, Inc. 1-ethyl-3-(3-dimethyl aminopropyl) carbodiimide (EDC) and N-hydroxysuccinimide (NHS) (98+%) were purchased from Alfa Aesar. Potassium ferricyanide, ferrocenemethanol, sodium lauryl sulfate (SLS), and citric acid were obtained from Fisher Scientific. Potassium chloride, concentrated sulfuric acid, hydroquinone (≥99%), poly (diallyl dimethylammonium chloride) (PDDA) (20 wt% in H_2O), hydrogen peroxide (30% wt in H2O), ABTS, and Tween-20 (0.06 mM @ 20-25 ^{O}C) were purchased from Sigma-Aldrich. Bovine Serum Albumin (BSA) (diagnostic grade) was obtained from Millipore. Sodium hydroxide and concentrated hydrochloric acid were obtained from VWR. Potassium chloride, potassium phosphate monobasic, sodium phosphate dibasic, and sodium chloride were procured from Acros Organics. Graphite pencil rod (HB, 0.5 mm dia., 60 mm long) was purchased from Walmart. Photopolymer B9R-4-Yellow resin was procured from B9Creations. Deionized water was passed through a Millipore Synergy UV water purification system to obtain 18.2 MΩ cm ultrapure water, which was used to prepare all solutions.

Printing of 3D Flow-through Device

Printing of the flow-through fluidic device was done according to previous reports.[7,39]

The fluidic device was designed using 123D Design CAD™ software (Autodesk) and fabricated

using a B9Creator v1.2 DLP projector-based SLA 3D printer.
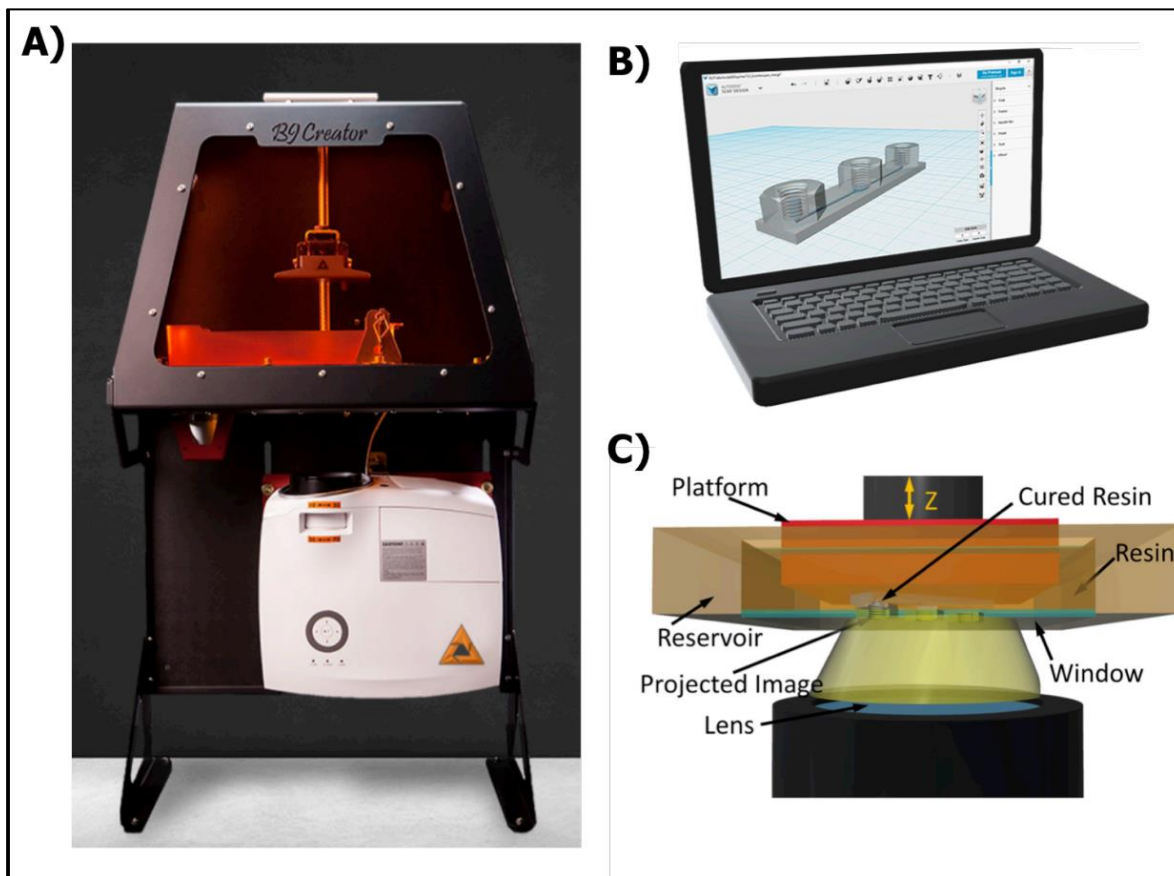
Figure 4. Photographic representation of B9Creator 3D-printer and the printing process. A) Picture of a DLP-based projector of 1.2v B9Creator B) A computerized representation of the fluidic device fabricated with computer-aided design (CAD) software. C) Illustrated representation of SLA printing with DLP-based projector during printing[7]

Fabrication of Electrode

Disk-shaped electrodes were made by integrating metal wires and graphite rods into

commercially available fittings as described previously.[46,47] These electrode fittings can be

incorporated into the 3D-printed fluidic device through threaded ports as in previous reports by

Bishop et al.[39] and Erkal et al.[40] Each fitting consisted of three working electrodes made using

pencil graphite rods, a reference electrode made from 0.25 mm diameter silver wire coated with

silver chloride, and a counter electrode fashioned from the barrel of an 16G stainless steel

needle. These electrodes were centered at the bottom of the fitting at equal distance to the ring-

shaped counter electrode which had the reference electrode placed inside it. The space between

the electrodes was filled with epoxy. After curing, the epoxy was polished to expose the

electrodes (Figure 5).
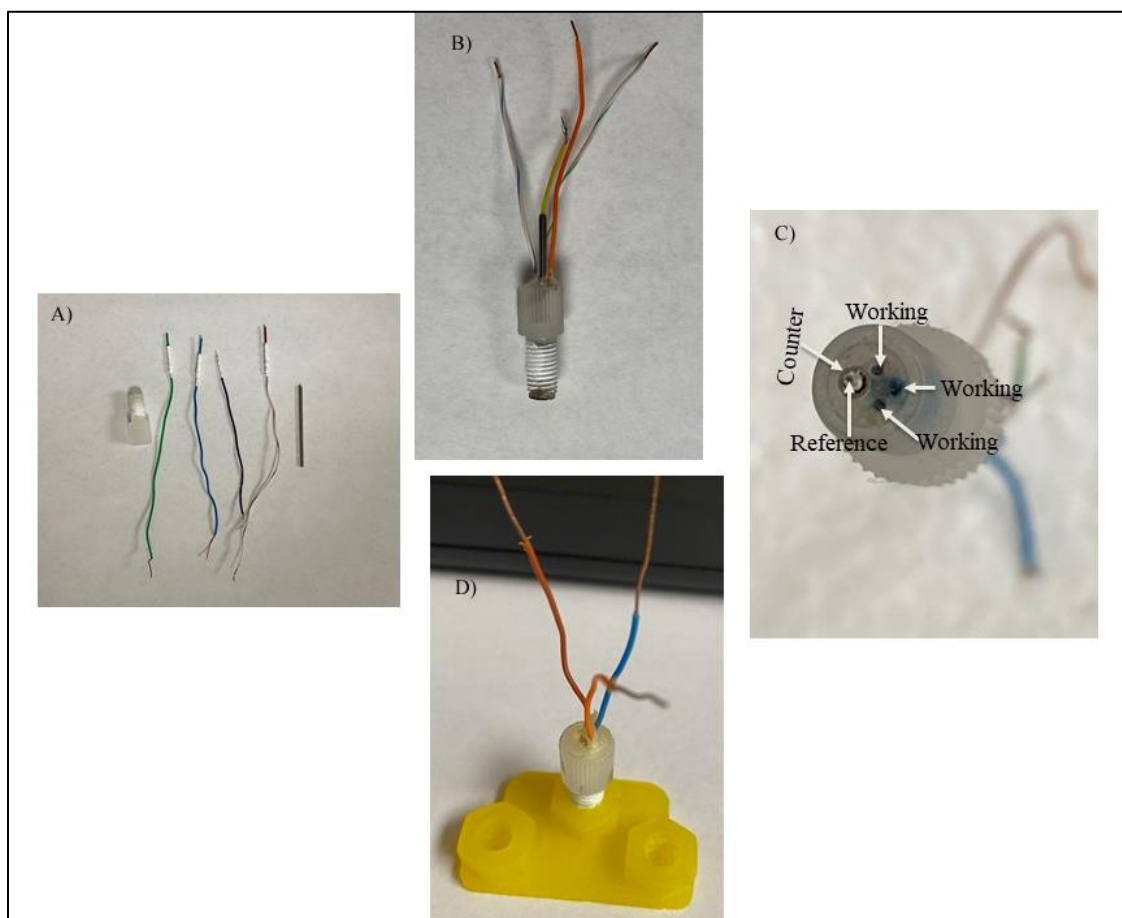
Figure 5. A complete photographic representation of the electrode fabrication process. A)
Individual electrodes with commercially available fitting. B) integrated electrodes into the
fitting. C) Image of fitting from below D) incorporation of fitted electrodes into a 3-D printed
microfluidic device

For carbon working electrodes, graphite pencil rods (0.5 mm diameter) were connected to copper wire by using a conductive silver paste and subsequently insulated using Teflon tape to avoid shorts to neighboring electrodes. The ring-shaped counter electrode was prepared made from the barrel of a stainless-steel needle. The reference electrode was fabricated by wrapping a silver wire around the copper and gluing them together using a conductive paste. The reference electrode was then insulated using Teflon tape to cover the silver wire-copper wire junction to prevent coming into contact with the counter electrode when placed in the barrel of the stainless-steel needle. Prior to the insertion of all individual electrodes into the fitting, the resistance of the electrodes was checked using a multimeter. The silver paste provided electrical connection to the electrodes with a low resistance of 0.9 Ω. After insertion of electrodes into fittings and polishing, resistance was checked again as negligent manipulation of electrodes can cause disconnection or electrical shorting. The conductivity of the electrodes was checked by hooking both ends of the electrode to a multimeter and to another electrode to ensure the electrodes are not in contact with each other. The copper wire provides connection of the electrode to the electrochemical instrument for measurements.

Electrochemical Measurement of Fabricated Electrodes

After the fabrication of electrode fittings, electrode polishing and conductivity checks, the reference electrode was coated with silver chloride to provide the system with a quasi-reference electrode.[46,68] This was done by placing the assembled electrode fitting in a 3.5 M KCl solution and connecting the reference electrode lead to the anodic part of a 9 V battery using 1.0 MΩ resistor embedded copper wire. The cathodic part of the battery was connected to silver chloride coated silver wire place in the same 3.5 M KCl solution to complete the circuit. This was allowed to stand for a minimum of thirty minutes until silver wire appeared gray after which

the open-circuit potential of the wire was measured in 1 M KCl against a commercial CH

instrument Ag/AgCl reference electrode (1 M KCl filling solution). Open circuit potentials were

found to be between 0 to 9 mV, indicating that silver chloride was successfully deposited on the

silver wires. To evaluate the performance of the electrode fittings, cyclic voltammetry was

performed using 8-channel CHI1040C electrochemical analyzer. Amperometry was performed

with the CHI1040C to carry out the electrochemical immunoassay.

Electrochemical Immunoassay

The electrochemical immunoassay strategy was adapted from previous work and reports

by Prof. Jim Rusling's group,[3,13,33-36] which are based on capture antibody-modified glutathione

(GSH)-capped gold nanoparticle (AuNP)-decorated screen-printed carbon electrodes and a

magnetic microbeads that are heavily labeled with an enzyme (HRP) and detection antibody for

biomarker protein isolation and signal generation. The same general strategy is employed here,

except electrode fittings and graphite working electrode arrays are employed in place of screen-

printed electrodes, and a 3D-printed fluidic device is used in place of simple PDMS-based fluidic

channels.

The electrode fitting featuring antibody-modified GSH-AuNP graphite working

electrodes is integrated into the 3D-printed fluidic device. The magnetic microbeads are

functionalized with streptavidin, which enables the attachment of commercially available

biotinylated antibodies and enzyme labels for electrochemical detection. Sample containing all

the three biomarkers (CA 125, OPN, MK) is exposed to labeled magnetic bead where each

specific detection antibody isolates its biomarker (CA 125, OPN, MK) of interest. The labeled

biomarker is introduced onto the antibody-coated nanostructured electrode via an injection

system, where the specific capture antibody on the electrodes forms a sandwich link with its

specific biomarker. Electrochemical detection is achieved by using hydrogen peroxide to activate the iron (III) center of the HRP label into a ferryloxy form, which reacts with an oxidizable species (e.g., hydroquinone) to produce an electrochemically reducible product (e.g., benzoquinone). A signal is generated in the form of current as the benzoquinone (formed from the reaction of hydroquinone with the activated enzyme) is electrochemically reduced back to hydroquinone when an appropriate potential is applied to the working electrode (Figure 6).
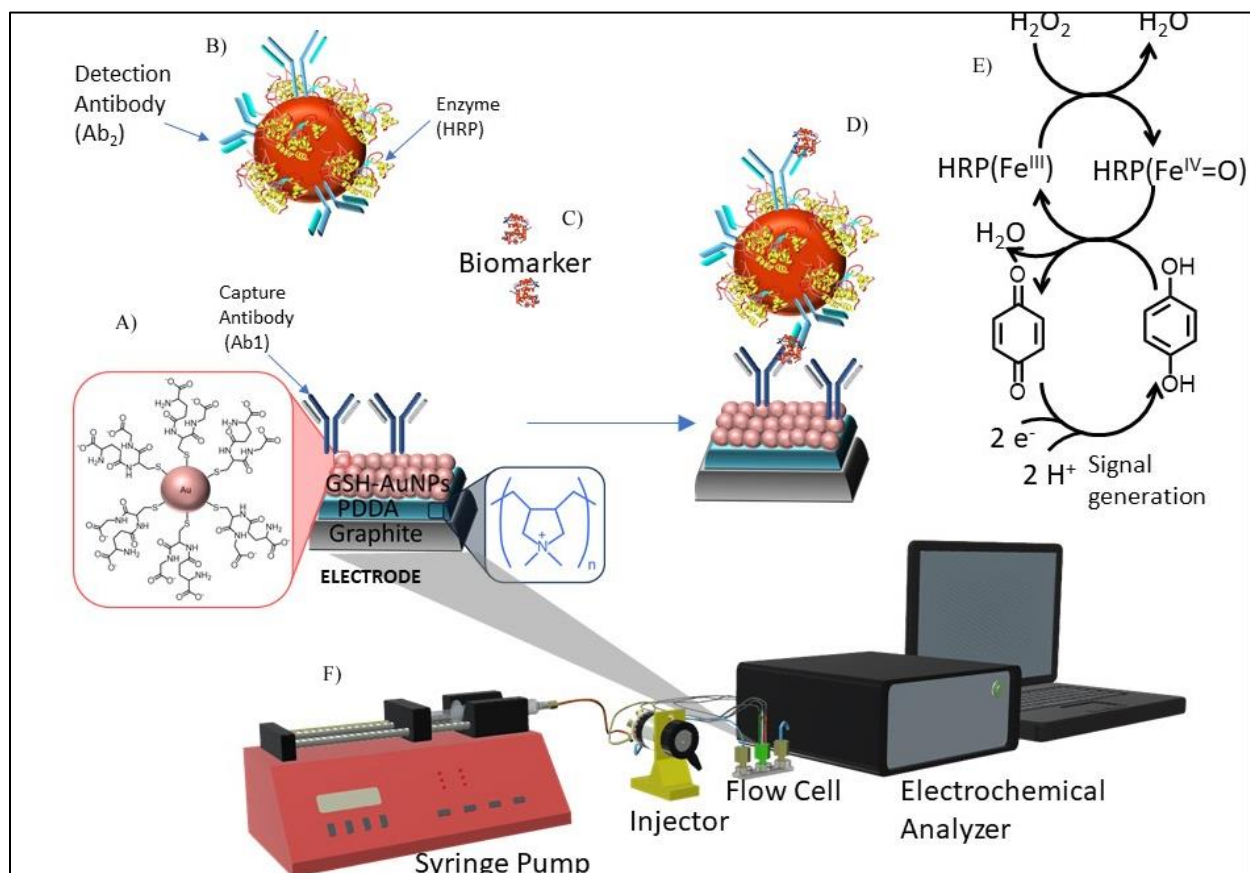
Figure 6. Illustration of the electrochemical immunoassay sensing strategy.A) Antibody modified GHS-AuNP graphite electrode. B) Magnetic bead functionalized with streptavidin to enable the covalent attachment of detection antibody and enzyme (HRP) label. C) Isolation of biomarkers with the magnetic bead bioconjugate. D) introduction of labeled biomarker onto the electrode surface for signal generation. E) Achievement of electrochemical detection through hydrogen peroxide oxidation of HRP and subsequent signal development by reduction of benzoquinone to hydroquinone. F) Set up for the biosensing system involving syringe pump for introducing reagent in the system, an injector for labeled biomarker conjugate introduction onto the electrode

surface placed in the fluidic device, and electrochemical analyzer for a signal potential generation

Electrode Modification with GSH-AuNP and Capture Antibody

Glutathione capped gold nanoparticles (diameter ~4 nm) were synthesized and characterized according to previously reported protocols.[32,36] Gold nanoparticles were deposited onto the graphite electrode via layer-by-layer electrostatic adsorption using a cationic polymer PDDA (Figure 7) followed by attachment of capture antibody through EDC/NHS amide bond formation. After deposition of GSH-AuNP onto the electrodes, cyclic voltammetry was performed in 500 mM sulfuric acid at a potential of -0.2 V to 1.5 V at 100 mV/s for 6 sweep segments to confirm presence of AuNPs.
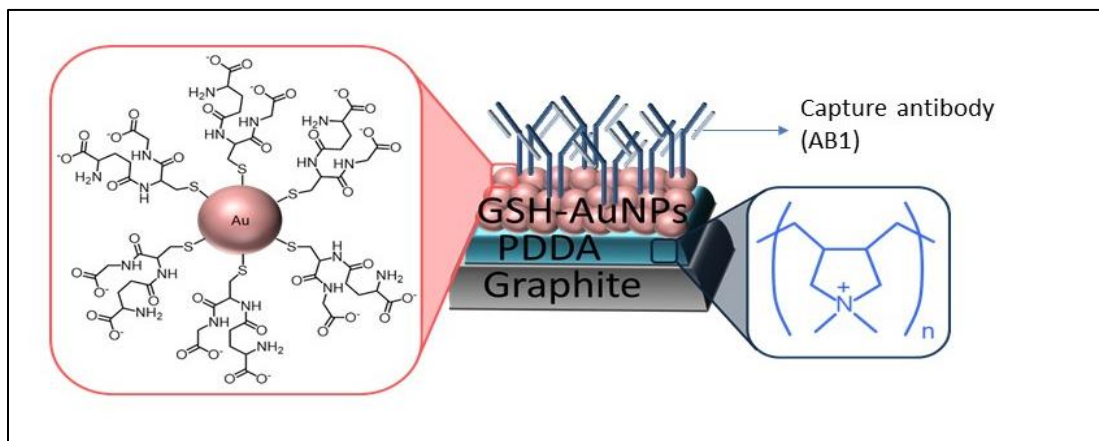
Figure 7. Layer-by-layer electrostatic adsorption modification of electrode with GSH-AuNP and capture antibody

Fabricated electrodes were rinsed with purified water, dried with nitrogen gas after which ~0.5 µl of 2 mg/ml PDDA was deposited and allowed to sit overnight. After performing CV, washing, and drying with nitrogen gas, a 0.5 µl of GSH-AuNP was drop cast onto the electrodes and allowed to sit overnight. A mixture of 0.5 µl EDC/NHS (~374 mM/~750 mM) was

deposited on the AuNP modified electrode and allowed to sit for 10 minutes after rinsing and drying the electrode. This was done to activate the carboxylate groups of glutathione for the attachment of capture antibody. Capture antibodies were prepared to the desired concentration. 0.3 µl of capture antibodies were carefully placed on each working electrode in the fitting, making sure that different capture antibody solution does not mix and keeping track of which electrodes have been modified with which antibody. Antibody-GSH-AuNP modified electrodes were then covered and incubated in the fridge overnight.

Preparation of Magnetic Bead-Antibody (Ab$_2$)-Enzyme (HRP) Bioconjugate

Following previous works and reports published by Malhotra et al.26, Chikkaveeraiah et al.[32], Krause et al. [36], and guidance from the manufacturer of magnetic beads (MBs) employed in these studies[69], HRP-MB-antibody (Ab$_2$) bioconjugates were made by first modifying magnetic beads with antibodies, followed by HRP. Briefly, 20 µl streptavidin-coated MBs (0.2 mg) were washed three times using 200 µl of 0.1 M phosphate buffer saline (PBS, pH 7.4). The MB suspension was vortexed and separated from wash buffer (PBS) with the aid of a 3D- printed tube holder magnetic bead separator. The separated pellet was resuspended in a 400 µl wash buffer to give a MB concentration of 0.5 mg/ml after the final wash. The HRP-MB-Ab$_2$ bioconjugate was optimized by varying the concentrations of Ab$_2$ (20 µl, 10 µl, 5 µl of 6 µg/ml) while amounts of HRP (15 µl of 0.25 mg/ml) and MB (50 µg) were constant. First, 100 µl of MB was modified with the varying volumes of Ab$_2$. For consistency, the volumes were brought to a total of 120 µl with PBS, votexed and placed on a rotator of 45 mins. MB-AB$_2$ were resuspended in 100 µl PBS after washing (3x) and vortexing. After modification of MB with Ab$_2$, MB-Ab$_2$ was mixed with 15 µl of HRP , vortexed and placed on a rotator (Figure 8) for 45 minutes. Beads

were separated from the solution and washed 3x with 100 µl of PBS and resuspended to a final

concentration of 0.5 mg/ml in 0.1 M PBS
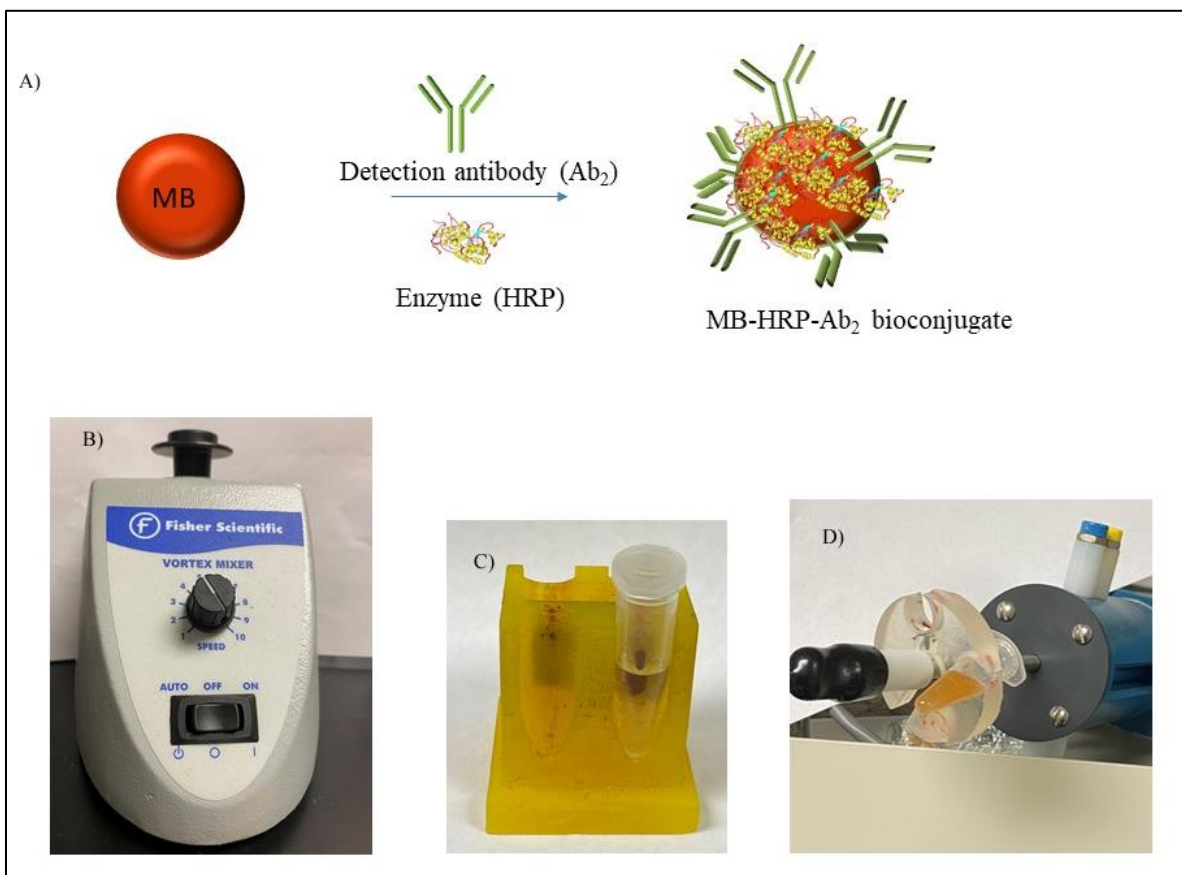
Figure 8. Illustration and photographic representation of the bioconjugation process. A)
preparation process of MB-HRP-AB₂ bioconjugate. Mixing of MB with reagent with vortex A)
followed by separation of MB from wash buffer using magnetic separator B). HRP and AB₂ bind
together on MB when placed on rotator D) for some time

Characterization of HRP Activity on Bioconjugate Using ABTS Assay

Active HRP content on modified magnetic bead was measured by performing an 2,2'-

azino-bis (3- ethylbenzothiazoline-6-sulphonic acid) (ABTS) assay using an optical density plate

reader. HRP standards ranging from 2 ng/ml to 100 ng/ml were made by diluting stock biotin-

HRP solution (2.5 mg/ml) in a 0.01 M PBS. Magnetic bead bioconjugates were diluted 160x

with 0.1 M PBS and 10 µl of each standard and samples were placed in the wells of the plate. To this, 150 µl of 1mg/ml ABTS in 100 mM phosphate citrate buffer (pH 5.0) with 0.03% hydrogen peroxide was added. This was incubated at room temperature for 30 minutes. To each well containing sample and standards, 100 µl of 0.6% SDS/SLS solution was added to stop reaction. With a recommended wavelength of 420 nm and a blank solution consisting of 150 µl phosphate-citrate in 100 µl 0.6% SDS/SLS, optical density measurement was taken at 420 nm wavelength with a background wavelength set at 600 nm.

Isolation And Labeling of Biomarker

For isolation and labeling of biomarker proteins from the sample during electrochemical immunoassays, three sets of HRP-MB-Ab_2 bioconjugates were prepared as described above using different antibodies (CA 125, OPN, MK) since each biomarker requires a different detection antibody. Magnetic beads with different Ab_2 labels were mixed, vortexed, washed separated, and resuspended in 0.1 M PBS to a final concentration of 0.5 mg/ml. To MB biconjugates, 30 µl of the solution was added to 10 µl of sample or control (PBS). The solution was then vortexed and placed on a rotator for 20 minutes at 400 RPM. After completion of labeling incubation period, the liquid portion of the solution was separated from magnetic beads by washing it 3x with 0.1 M PBS as described above. Beads were finally resuspended in 60 µl PBS and kept in the fridge or ice prior to analysis.

Flow-Injection System

Prior to electrochemical signal development, the antibody-modified electrode was obtained and inserted into the fluidic device while the labeled biomarker bioconjugate was left to incubate. The obtained electrode was rinsed in 0.1% Bovine Serum Albumin (BSA) in PBS. This was done to reduce non-specific binding on the electrode and in the flow cell. The electrode was

36

inserted into the central port of the 3D printed flow cell. This was carefully done as overtightening could break and destroy the flow cell. To improve sealing with into 3D printed threaded port, the threaded part of the electrode fitting was wrapped with Teflon tape. An inlet tubing was inserted into one of the threaded ports which had been secured with commercially available fitting. The tubing was connected to the outlet of a manual injector (Rheodyne, LLC) that featured a 20 µl sample loop and inlet connected to a syringe pump (New Era Systems) to complete the flow-injection system. This system (figure 9) is designed to aid in the delivery of reagents, samples, and control onto the electrode surface through the channel for electrochemical measurement. An optimized flow rate of 100 µl/min was used for amperometry.
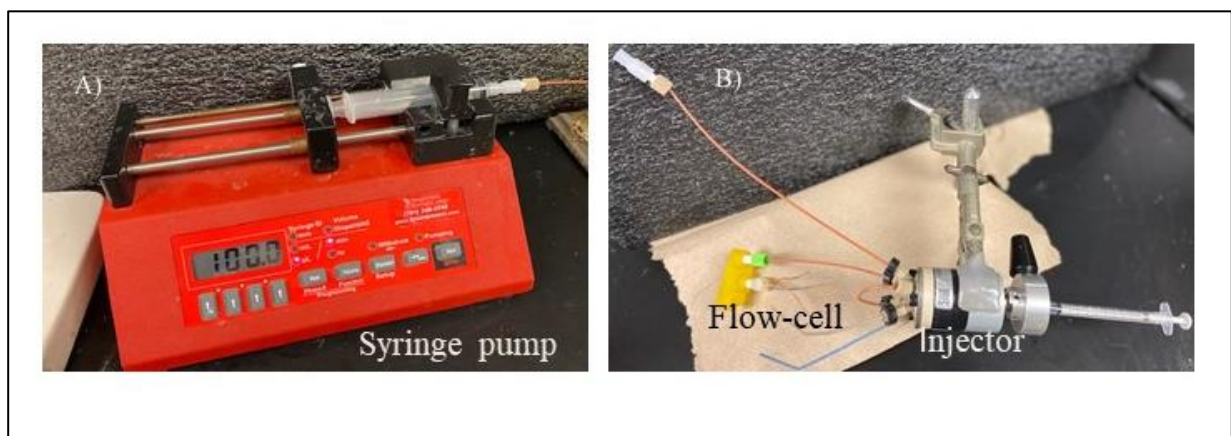
Figure 9. Photographs of the flow-injection system. A) Photograph of the syringe pump at 100 µl/min. B) Photograph of an injector connected to a fluidic device with incorporated electrode through the inlet tubing

Capture of Labeled Biomarker and Electrochemical Signal Development

For capture of antigen-Ab_2-MB-HRP onto electrodes, 60 µl of 1% BSA in PBS was loaded and injected into the sample loop with 0.05% Tween-20 in PBS drawn in a syringe to facilitate the flow of BSA onto the electrode surface and through the flow-cell channel. This was done to reduce non-specific binding in the flow cell and on the electrode surface. Upon the arrival of BSA on the electrode surface after 40 seconds, the flow was stopped to allow

incubation of BSA on the electrode surface for 5 minutes. The flow was resumed and, with the injector lever in the load position, 60 µl of beads were carefully loaded into the sample loop. The beads were injected into the fluidic device at a rate of 100 µl/min by moving the lever of the manual injector into the inject position. The flow was stopped once beads reached the electrode and incubation carried out under stopped-flow for 10 minutes. The flow was resumed at 10 µl/min for 8 minutes followed by 100 µl/min for 3 minutes to ensure enough time for beads to bind and completely remove excess beads.

For signal development, 1.0 mM hydroquinone solution in the syringe was allowed to flow through the system at 100 ul/min for about 2 minutes. An appropriate potential was applied to the electrode using an i-t method in the electrochemical analyzer software. After the decay of background current to near zero for about 100 seconds, a mixture of 100 µM hydrogen peroxide in 1 mM hydroquinone was carefully loaded into the sample loop and injected to activate HRP label present on magnetic beads. Signal which is proportional to the concentration of biomarkers present in the sample was provided by the reduction of benzoquinone (oxidized hydroquinone) back to hydroquinone.

Enzyme-Linked Immunosorbent Assay Measurement

ELISA measurement was done based on protocol provided by the Duoset manufacturer (R&D Systems). Capture antibody was diluted to working concentrations using PBS. A 96-well microtiter plate was coated with 100 µl of the capture antibody, sealed and allowed to incubate overnight at room temperature. Wells were then washed with 400 µl wash buffer and plate blocked with 300 µl reagent diluent to prevent non-specific binding for 1 hour. Aspiration and washing were performed after plate blocking process.

To each well of the titer plate, 100 µl of sample or standards in reagent diluent was added. The plate was then covered with an adhesive strip and allowed to incubate for 2 hours. Aspiration and washing step were repeated after the 2 hours incubation period. To each well, 100 µl of detection antibody, diluted to working concentration in reagent diluent was added, covered, and let to incubate for 2 hours. Aspiration and washing steps were repeated. Following this, 100 µl of streptavidin HRP was added, plate covered and incubated for 20 minutes. Aspiration and washing steps were performed which followed addition of 100 µl substrate solution, incubated away from light for 20 minutes. Finally, a 50 µl stopping solution was added to the substrate solution and gently mixed thoroughly for optical measurement at a 450 nm wavelength using 540 nm wavelength as background correction.

CHAPTER 3. RESULTS AND DISCUSSIONS

Electrode Characterization

Electrochemical signal is largely dependent on the activity or behavior of the electrode. The electrochemical behavior of pencil graphite working electrodes was evaluated using cyclic voltammetry. Electrode fittings were placed in a solution of 0.1 M KCl (supporting electrolyte) with 0.5 mM ferrocene methanol (FcMeOH) as the redox probe. In this solution, a pair of peaks centered at 198.0 ± 5.0 mV (n=20) vs. Ag/AgCl reference electrode was observed, which is consistent with the one-electron oxidation of ferrocenemethanol and subsequent reduction. The separation between the anodic and cathodic peaks was found to be 65.0 mV, ranging from 55mV to 77.0 mV. Although the peak separation is slightly higher than the expected Nerst faradaic potential (59 mV) for a one electron reversible redox system, the obtained value of 65 mV is in good agreement with reported values for other carbon-based electrodes for a reversible electron transfer system,[7,70-77] which confirms the pencil graphite working electrodes are suitable for electroanalytical measurements.

Pencil graphite working electrodes are composed of a mixture of graphite, clay, and a polymeric binder. The ratio and distribution of these components can vary at the electrode surface, which can affect faradaic current measurements.[70,72-75] Therefore, the electroactive surface area (i.e., the area of the electrode that can participate in electron-transfer reactions; also known as the real surface area) of each electrode was determined by applying the Anson equation[76] (Eqn. 1) to chronocoulometric data obtained from the oxidation of 0.5 mM ferrocene methanol in 0.1 M KCl at an applied potential of 350 mV.

$$Q = Q_{dl} + Q_{ads} + 2nFA_eC \left(\frac{Dt}{\pi}\right)^{1/2} \qquad (1)$$

where Q is the charge (in C), Q_{dl} and Q_{ads} are charges associated with double-layer

charging and Faradaic reactions of adsorbed species, n is the number of electrons transferred

during electrochemical redox reaction, F is Faraday's constant (96,485 C/mol), A_e is the

electroactive surface area (in cm^2), C is the concentration of redox probe (i.e., FcMeOH) (in

mol/cm^3), and D is the diffusion coefficient of the redox probe (7.80×10^{-6} cm^2/sec).[77]

Using equation 1 the average electroactive surface area based on twenty electrodes was

4.5 ($\pm$ 2.4) x 10^{-3} cm^2 (n=20). The geometric surface area that is expected for graphite pencil with

0.5 mm diameter and 60 mm long is 2 x 10^{-3} cm^2. The electroactive surface areas of pencil

graphite electrodes have generally been reported as larger than their corresponding geometric

areas (e.g., 0.255 cm^2 for a 0.5 mm HB-type pencil[78], 3.1 x 10^{-3} cm^2 for 0.5 mm pencil[7]). Large

electroactive surface areas help facilitate measurement of low concentrations of analytes.[79] The

variations observed between the electroactive surface area of the electrodes and the geometric

area may be attributed to the roughness of the electrode surface and variations the cross-sectional

shapes due to the positioning of electrodes in fitting during electrode fabrication. Current

generated at each electrode was normalized by the electroactive surface area (Figure 10 C-D) to

account for differences in response that can be attributed to differences in electrode size.
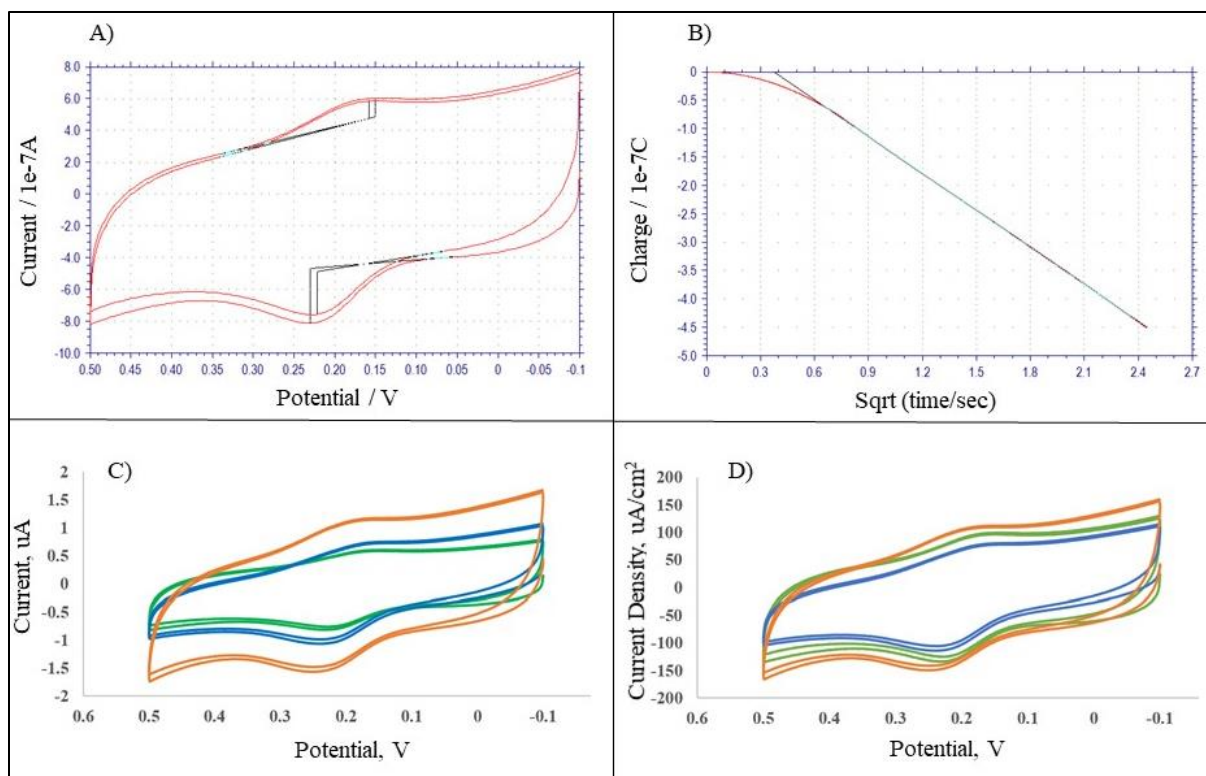
Figure 10. Electrode characterization and surface area estimation. A) Illustrated CV response for an electrode in a fitting showing redox peak response centered at 198.0 mV vs Ag/AgCl with peak separation of 65 mV. B) Illustrated chronocoulometric response for electrode showing the slope used in the Anson's Equation. C) CVs of raw currents of 3 working electrodes in a fitting. D) CVs of current density of 3 working electrodes in a fitting

Since electrochemical sensing during immunoassay experiments is performed in a 3D-printed fluidic device, the electrochemical behavior of the electrode fitting in the flow-cell was ascertained using CV and compared to CV measurement obtained for the electrode fitting when placed in a beaker. Using hydroquinone (since it is the electrochemical oxidizable species for sensing) as the redox probe, CV measurement was repeated for electrode in and out the fluidic device to compare their electrochemical response.

The results obtained for both in and out the fluidic channel did not show any significant differences in the peak current and peak position for electrode (Figure 11). This confirmed that

electrochemical sensing can be reliably and successfully performed in the 3D printed fluidic device with low-cost graphite electrodes incorporated.
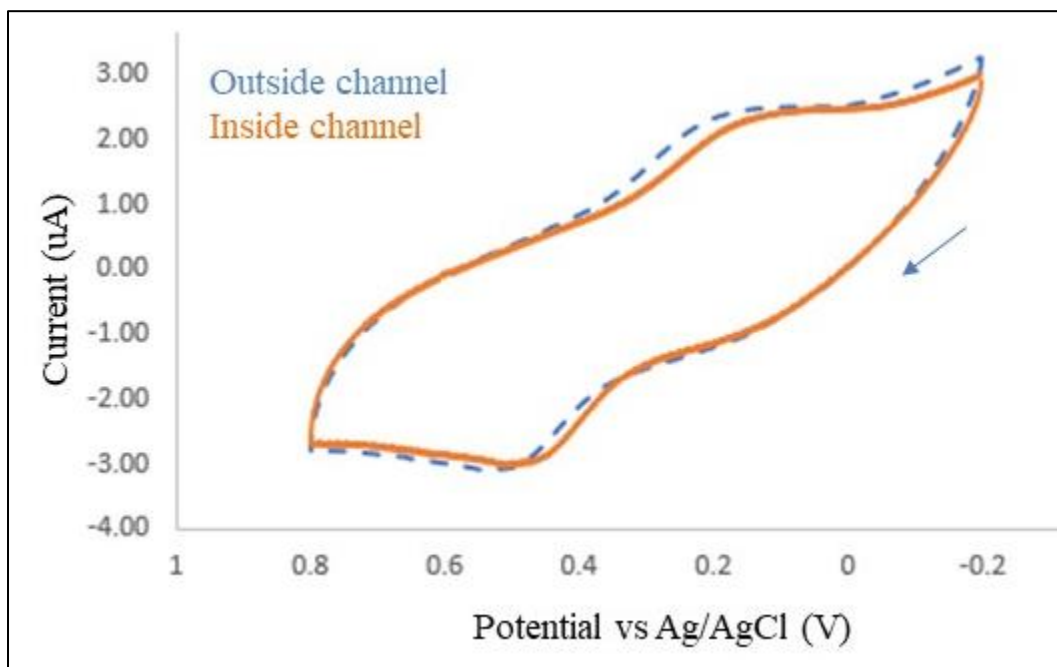
Figure 11. CV responses of electrode fitting inside and outside the fluidic channel towards a 1.0 mM hydroquinone redox at a scan rate of 100 mV/s. Arrows indicate the scan direction

Flow-through Amperometry

The sensing system (Figure 9) involves the introduction of reagents, samples into the fluidic device, incubation periods and washing step. Therefore, it is of extreme importance to establish when reagents reach the electrode surface in the flow cell upon injection. A 20 µl mixture of potassium ferricyanide $K_3[Fe (CN)_6]$ (1.0 mM) in 0.1 M KCl (supporting electrolyte) was injected under a 100 µl/min flowrate at a constant potential at which potassium ferricyanide is reduced to potassium ferrocyanide (0 V vs. Ag/AgCl). Once the redox probe reached the electrode surface, a peak-shaped response appeared after an average time of 40.15 ($\pm$ 0.75) s of injection (Figure 12). This generated an average current of 131 ($\pm$ 3.02) nA and a peak area of 3.021 ($\pm$ 0.068) µC. This implies that, flow injection could be stopped at ~40 s to allow reagents

and reactions such as non-specific binding, washing steps and incubation of MB bioconjugate to take place on electrode surface to ensure maximum binding of analyte to capture antibodies on the electrode surface.
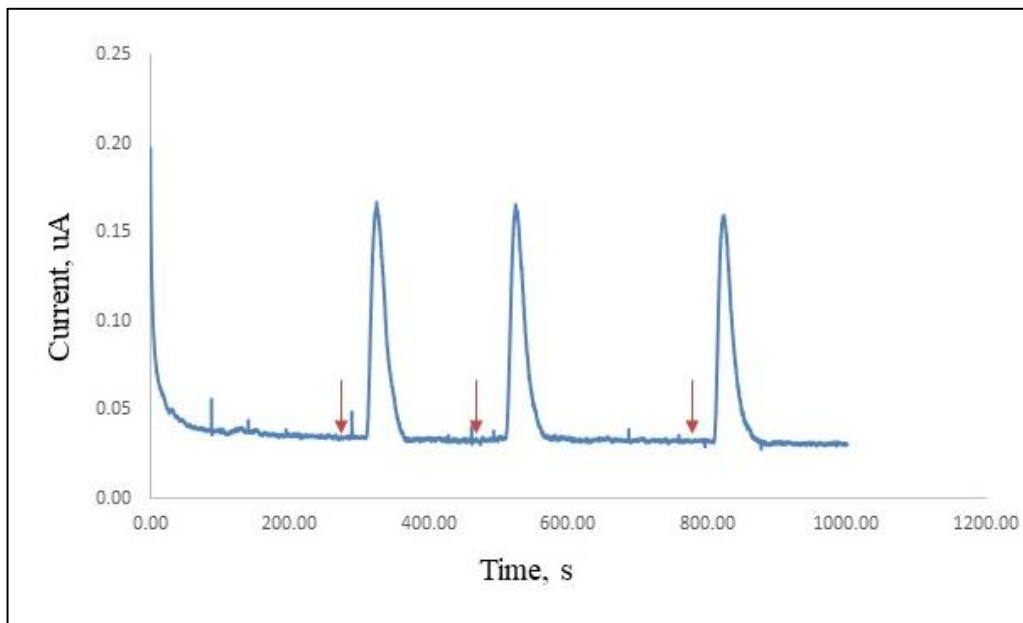
Figure 12. Flow-through amperometric signal for a 20 µl of 1 mM ferricyanide in 0.1 M KCl injected at 300 sec, 500 sec, and 800 sec under a 100 µL/min flow of 0.1 M KCl at a constant 0 V potential vs. Ag/AgCl

Electrode Modification and Characterization

Electrochemical immunoassay was developed by modifying the electrode surface with glutathione-capped gold nanoparticle (GSH-AuNP) and capture antibody. GSH-AuNPs were prepared and particle size estimated based on previous reports by Rusling et al. [32,34,35] The position of the surface plasmon resonance peak (A_{spr}) at 515 nm in the UV-Vis spectrum (Figure 13) is consistent with previous reports indicating the particles to be <25 nm in diameter.[80] In order to estimate particle size that is less than 25 nm by UV-Vis, the ratio of the absorbance at the SPR peak (i.e., Aspr) to absorbance at a 450 nm (A_{450}) is used as reported by Haiss et al.[80]

From the particles made, the ratio of Aspr to A_{450} was dtermined to be 1.19 and this corresponds to 4 nm.
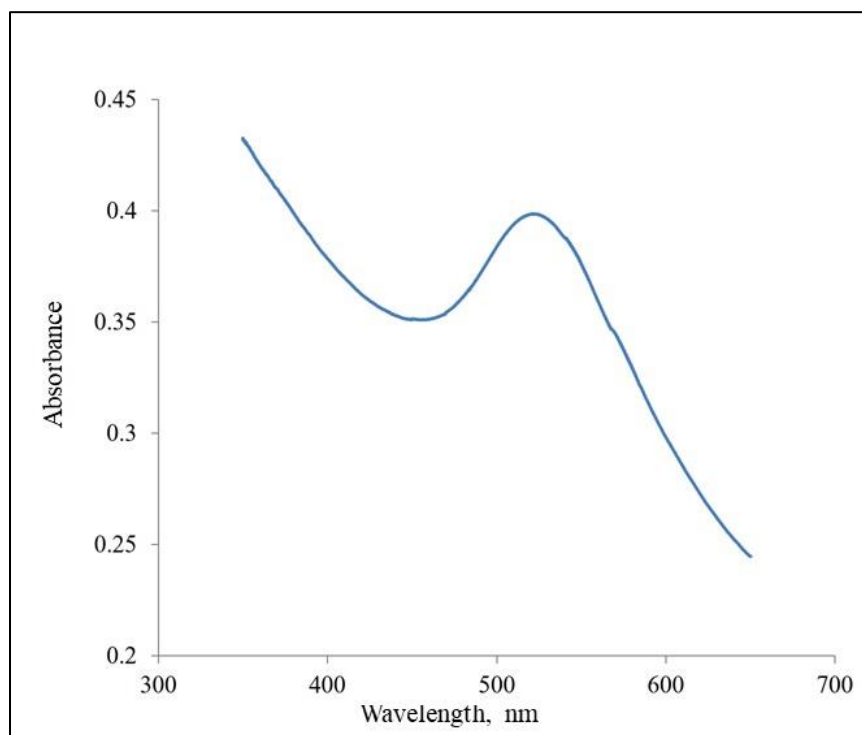
Figure 13. Peak position at 515 nm for a 4 nm GSH-AuNP on a UV-Vis spectrum

Using a layer-by-layer electrostatic adsorption strategy previoulsy employed for pyrolytic graphite[81] and screen-printed carbon[32,35,77] electrodes, GSH-AuNPs were adsorbed onto pencil graphite with the aid of a cationic PDDA polymer interlayer.[81] To confirm the successful deposition of AuNP on the electrode, CVs in 0.5 M sulfuric acid were performed on unmodified and modified electrodes in the potential window of -0.2 V to +1.5 V vs. Ag/AgCl. Within this range, surface gold is oxidized to gold oxide and on the return scan, reduced back to gold according to the following half-reaction[7]:

$$3H_2O + 2Au \rightleftharpoons Au_2O_3 + 6H^+ + 6e^-$$
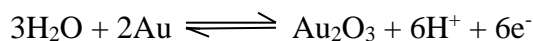
An anodic (oxidation) peak positioned at 1.2 V and a cathodic (reduction) peak at 0.65 V indicated the successful depostion of AuNP. This was compared to CVs of unmodified and

PDDA modified electrodes which showed no significant peaks (Figure 14). A mixture of EDC/NHS was used to activate the carboxylate functional groups on the AuNP in order to form amide bonds with amine groups on the antibodies (CA 125, OPN, MK).
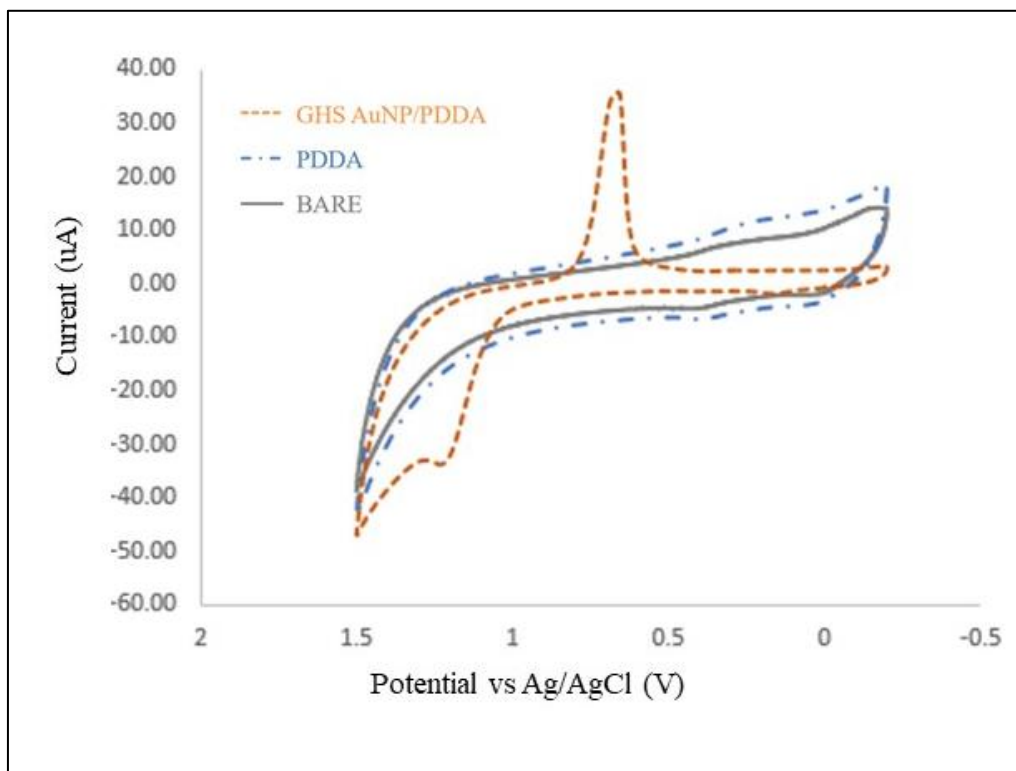
Figure 14. CVs at scan rate of 100 mV/s of bare, PDDA and AuNP-modified electrodes in 0.5 M H_2SO_4. Arrow shows the beginning of scan

Ab₂-MB- Hrp Bioconjugation and Characterization

For the optimization of HRP-MB- Ab_2 bioconjugate, the washed magnetic beads was portioned into four separate microcentrifuge tubes (0.05 mg MB per tube). To each centrifuge tube, varied amounts (0.12, 0.06, 0.03 µg) of biotinylated detection antibody was added. For consistency, all biotin-IgG detection antibody was brought to a total volume of 120 µl by adding PBS. A constant amountof HRP (3.75 µg) was added to all the Ab2-MB sololution, washed and resuspended at a final concentration of 0.5mg/ml in 0.1 M PBS.

46

To determine the amount of active HRP per magnetic bead, an ABTS assay was performed at an absorbance of 420 nm using standards concentration of HRP ranging 0 ng/ml to 100 ng/ml (Figure 15) to develop a calibration curve (Figure 16).
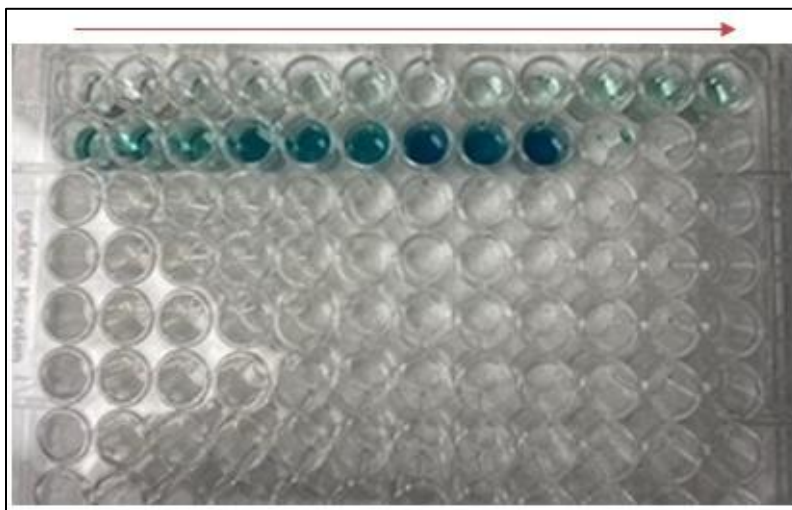
Figure 15. Microtitre plate showing concentrations (0 ng/ml to 100 ng/ml) of standard HRP with a mixture of 1 mg/ml ABTS in 100 mM phosphate citrate buffer and 0.03% hydrogen peroxide. Arrow direction indicate lower concentration to higher concentration
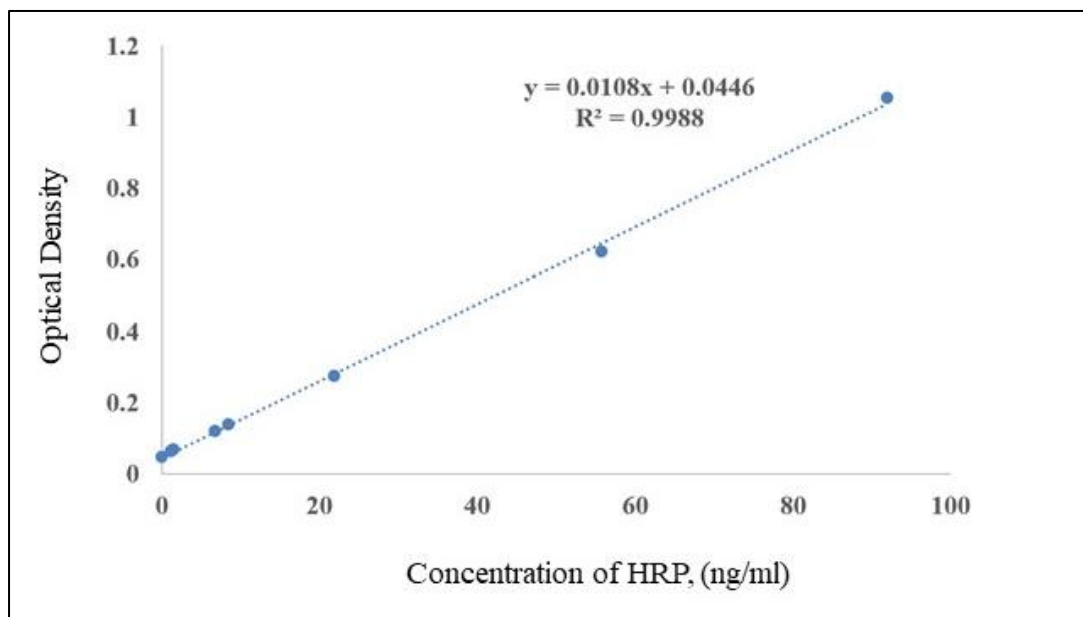
Figure 16. Calibration curve of HRP using ABTS assay

It was observed that there was a decrease in active HRP for bioconjugate with increased antibody on the MB during immobilization step (Figure 17). The estimated active HRP per MB particle was calculated to be in a range of ~20,000 to ~100,000. The range of active HRP obtained is in very close agreement with previously reported active HRP (~2 x 10^5) by Rusling et al .[34,35,36]
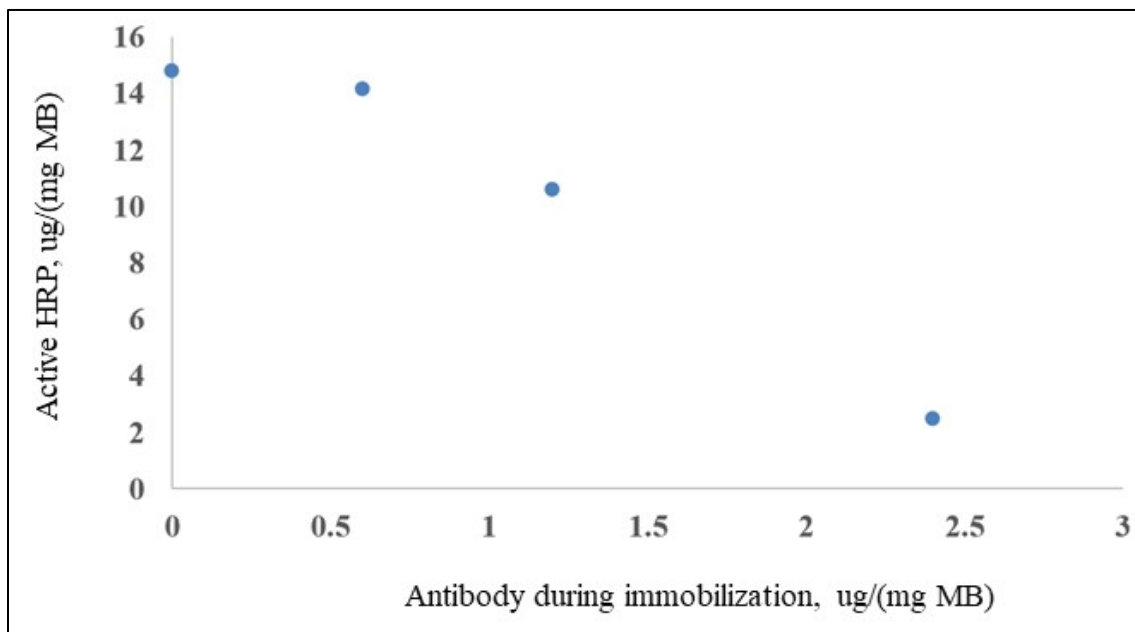
Figure 17. Active HRP per magnetic bead during functionalization

Signal is enhanced by the amount of HRP present on the magnetic bead, while a large amount of Ab$_2$ labels is necessary for effective capture of low concentrations of antigens.[82] Therefore, it is important to have an appropriate ratio of HRP to Ab$_2$ to enhance signal and push detection limit low. With no antibody on the MB (0 µg/mg MB), maximum binding of HRP was observed with ~100,000 active HRP. This had no significant difference when 0.6 µg of antibody were immobilized on the MB during bioconjugation and little HRP present (~20,000 active HRP) when amount of the antibody per magnetic bead was increased to 2.4 µg/ml MB. Having

observed this, 1.2 µg of antibody per mg MB was selected for the electrochemical assay since there were enough antibody to HRP present on MB.

Enzyme-Linked Immunosorbent Assay

Prior to the electrochemical immunoassay development, traditional ELISAs were performed on protein standards and pooled human serum samples. This was done to ascertain the level of quality of the commercially available duoset antibodies, which were also used to modify electrodes and magnetic beads for electrochemical immunoassays. Using a standard concentration ranging from 78.1 -5000 pg/ml for MK, 62.5 – 4000 pg/ml for OPN and 31.3 – 2000 pg/ml for CA 125, a four-parameter log fit (4-PL) calibration curves were generated for all biomarkers (Figure 18-20) with R^2 values of 0.998, 0.999, and 1 for MK, OPN, CA125 respectively.
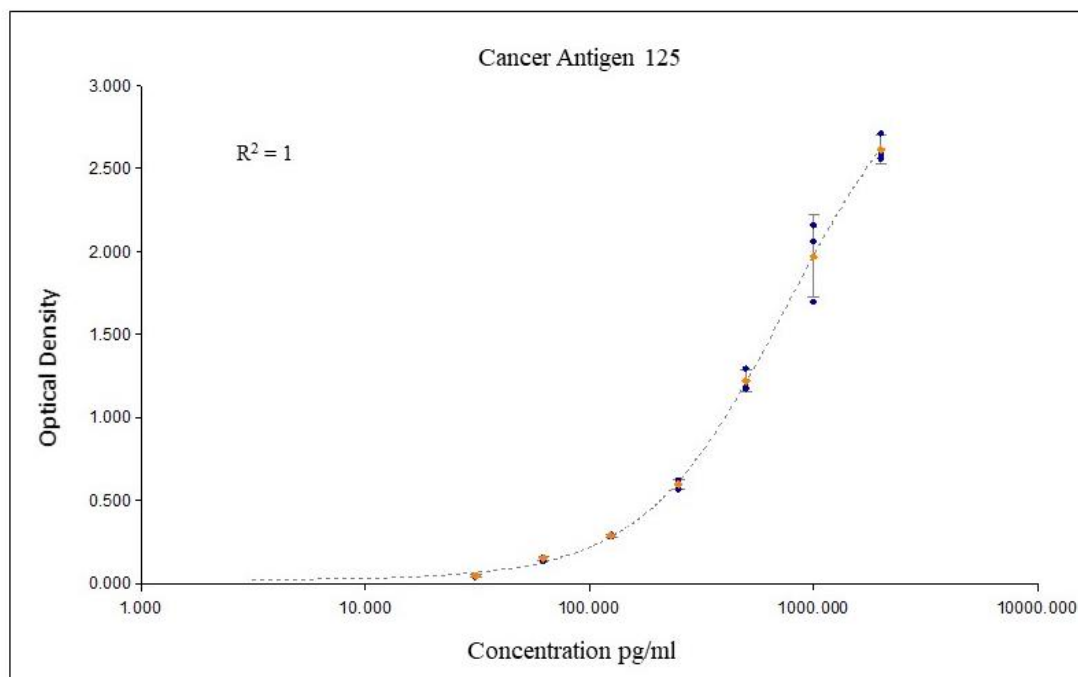
Figure 18. Illustrated calibration curve for standard Cancer Antigen concentrations ranging from 31.3 – 2000 pg/ml
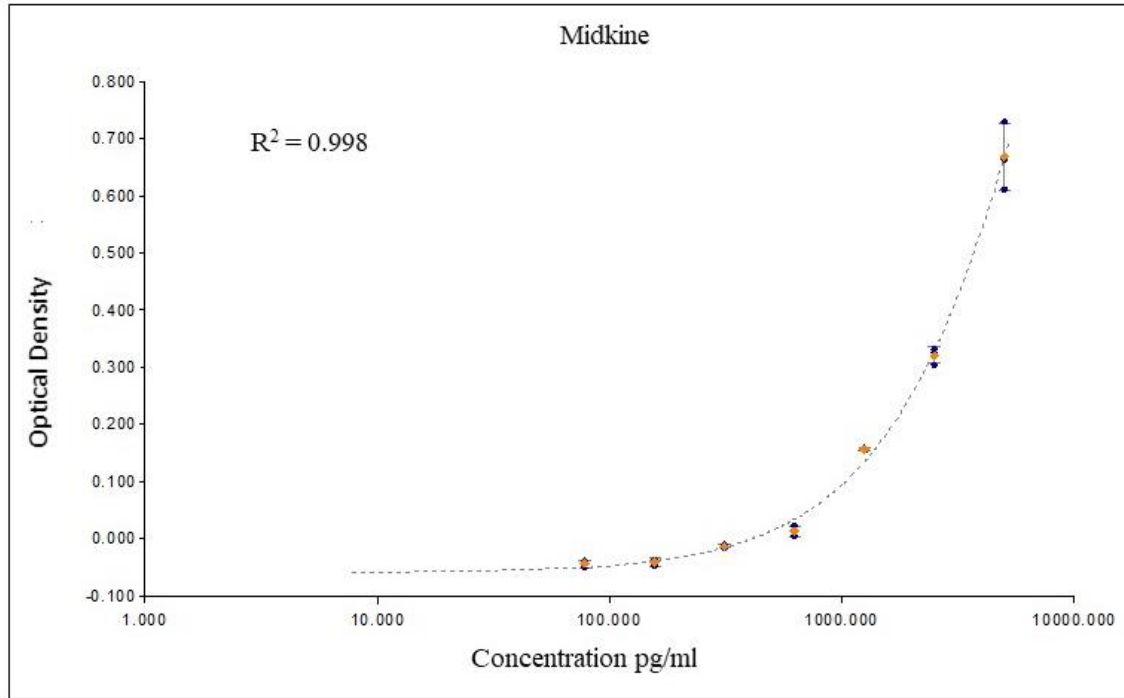
Figure 19. Illustrated calibration curve for standard Midkine concentrations ranging from 78.1 – 5000 pg/ml
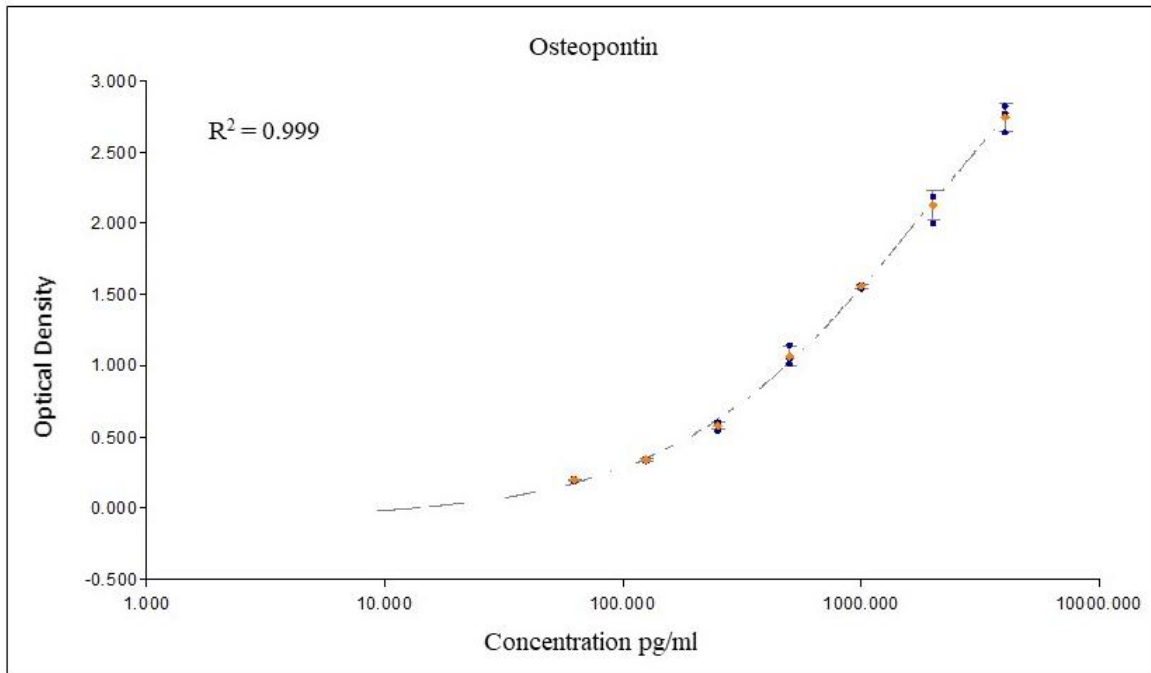
Figure 20. Illustrated calibration curve for standard Osteopontin concentrations ranging from 62.5 – 4000 pg/ml

To determine if the matrix of the human pooled serum sample is interfering or has any effects on the ability of the capture and detection antibody to bind with antigen, a spike and recovery test was performed. By spiking a known concentration of the various biomarker standards into the serum sample, percentage recovery ranged between 87.91 % to 106.91 % for CA 125, 82.58 % to 103.70 % for OPN and 88.52% to 98.09% for MK. In performing this type of assay (ELISA), measurement is said to have little or no matrix interference if percentage recovery is in the range 80 – 120.[83] This showed that the antibodies were in good condition and suitable for the electrochemical assay.

Table 2. Concentration and % Recovery for CA 125 Biomarker. Measured Concentration of Unspiked Serum was 247.9 (± 8.6), n=3

Spiked conc. (pg/ml)	Mean measured spiked conc. (pg/ml) / (±SD)	Mean % Recovery / (±SD)
70	62 (± 13)	88 (± 22)
350	374 (± 32)	106.9 (± 8.6)
700	672 (± 88)	96 (± 14)
1400	1335 (± 99)	95.3 (± 7.4)

Table 3. Concentration and % Recovery for OPN Biomarker. Measured Concentration of Unspiked Serum was 1886.1 (± 13.9), n=3

Spiked conc. (pg/ml)	Mean measured spiked conc. (pg/ml) / (±SD)	Mean % Recovery / (±SD)
100	96 (± 24)	96 (± 25)
750	620(± 57)	82.6 (± 9.2)
1500	1453 (± 104)	96.9 (± 7.2)

3000	3111 (± 113)	103.7 (± 3.6)

Table 4. Concentration and % Recovery for MK Biomarker. Measured Concentration of Unspiked Serum was 3557.6 (± 31.3), n=3

Spiked conc. (pg/ml)	Mean measured spiked conc. (pg/ml) / (±SD)	Mean % Recovery / (±SD)
80	79 (± 20)	98 (± 25)
800	710 (± 36)	88.5(± 5.1)
1600	1473 (± 50)	92.1 (± 3.4)
3200	3069 (± 53)	95.9 (± 1.7)

Concentrations obtained for the various biomarkers were in range with concentrations reported in literature.[66,67]

Electrochemical Immunoassay Signal Development

For electrochemical immunoassay development, standard mixtures of the three biomarkers (MK, OPN, CA 125) were introduced to a mixture of HRP-MB-Ab$_2$ bioconjugates. After incubation to label biomarker proteins with corresponding bioconjugate and subsequent washing to remove other proteins and materials, the bioconjugate-labeled protein mixture was injected into the flow-through system and onto the electrodes for capture and detection. A mixture of hydrogen peroxide and hydroquinone is introduced into the system to activate Fe (III) center of the HRP on the bead via oxidation. This activated HRP in turns oxidizes the hydroquinone into benzoquinone. Therefore, for electrochemical signal to be generated, a constant potential at which benzoquinone is reduced back to hydroquinone must be applied.

To determine the potential for the reduction of benzoquinone back to hydroquinone, CV

measurements were taken in 1mM hydroquinone with phosphate-buffered saline as the

supporting electrolyte. Hydroquinone was first oxidized to benzoquinone electrochemically and

on the return scan, reduced back to hydroquinone (Figure 21). A pair of redox peaks centered at -

30 mV with a peak separation of 64 mV were obtained from the voltammogram. From the

voltammogram obtained, a more negative potential of -0.20 V was selected for the

electrochemical signal development. This is due to the fact that, at that potential all the

benzoquinone had been completely reduced back to hydroquinone and so to avoid the onset of

current from other possible reactions while achieving a complete reduction of benzoquinone

generated from the enzymatic reaction, a potential of -0.20 V is appropriate to use.
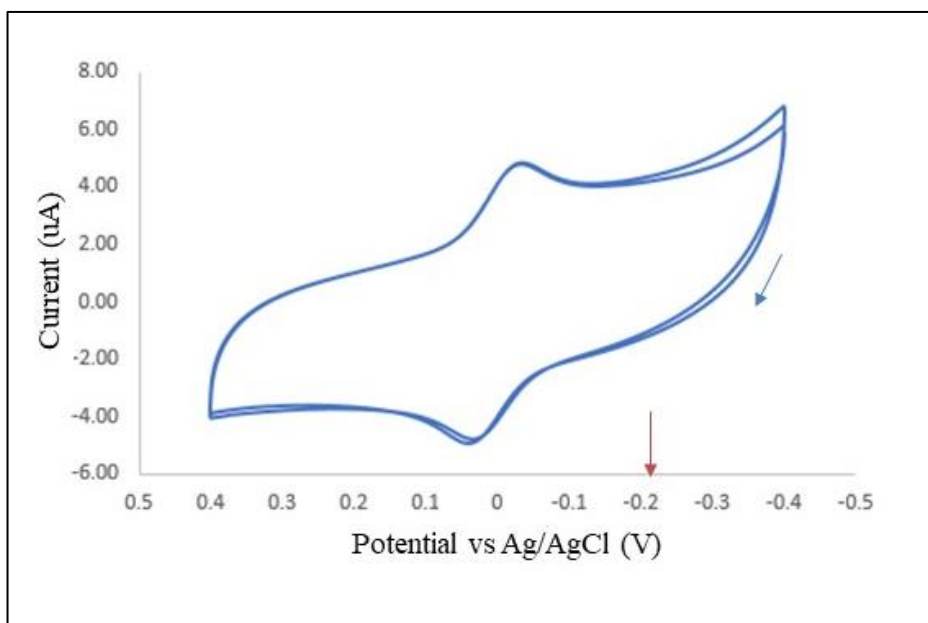
Figure 21. CV in a 3D-printed fluidic device for a 1.0 mM hydroquinone solution in 0.1 M PBS
at a 100 mV/s flowrate. Beginning of the scan is shown by the blue arrow. The red arrow shows
the potential (- 0.20 V vs. Ag/AgCl) used in the amperometric detection of reduced
benzoquinone

The fundamental principle for electrochemical signal development is the reduction of

enzyme-generated benzoquinone to hydroquinone. There it is possible to obtain a false positive

53

result for signal development if the hydrogen peroxide used in the activation of Fe (III) of the enzyme (HRP) can directly oxidized hydroquinone to benzoquinone or oxidize it electrocatalytically with the presence of AuNP on the electrode surface, since hydrogen peroxide is an oxidizing agent.

To confirm that signal generation is directly from the reduction of enzyme-generated benzoquinone (i.e., presence of HRP-MB-Ab$_2$), two amperometric detection was performed, where one test had HRP-MB-Ab$_2$ present and the other with no bioconjugate present (just pure water). Amperometric signal was generated only for the test with HRP-MB-Ab$_2$ (Figure 22). This confirmed that HRP-MB-Ab$_2$ is necessary for the oxidation of hydroquinone to benzoquinone and that hydrogen peroxide alone or with AuNP present, would not be able to oxide hydroquinone to benzoquinone.
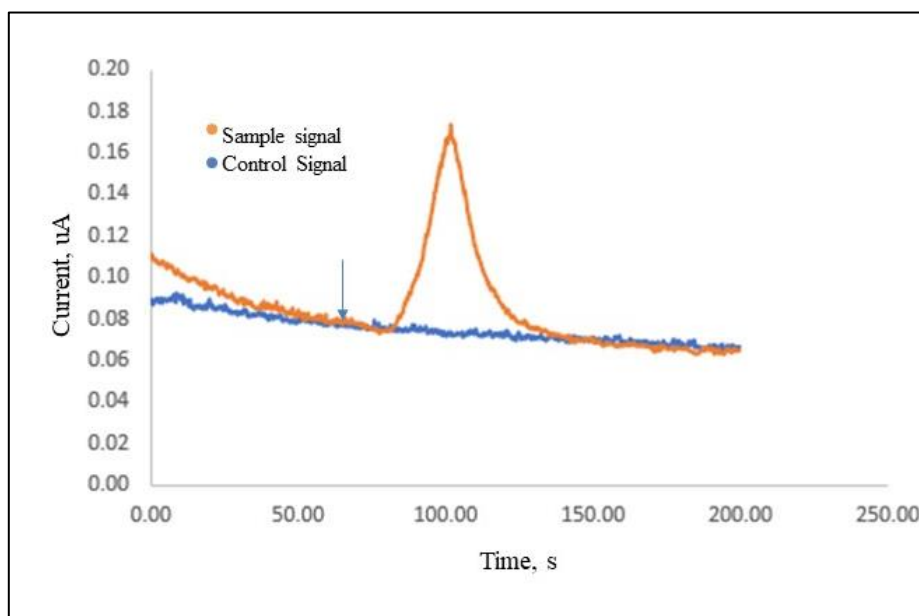
Figure 22. Amperometric response generated to compare in the absence and presence of Ab2-MB-hrp bioconjugates. For Control signal generation, electrode was exposed without CA 125 and MB bioconjugates (only purified water). For Sample, electrode was exposed to 0.31 pg/ml sample conjugated with MB bioconjugate. Signal was developed by injecting a 1 mM hydroquinone with 0.1 mM H2O2 at a flowrate of 100 µL/min. Arrow indicates sample injection time at an applied potential of -0.20 V vs. Ag/AgCl

54

To demonstrate that immunoassay signal is related to the concentration of antigen, mixtures containing MB bioconjugates for the 3 different proteins (CA 125, OPN, and MK) were added to standard solutions containing 0 pg/mL (control), low concentrations (100x lower than lowest reported concentration for commercial ELISA), and moderate concentrations (equal to the lowest reported concentration for commercial ELISA) of CA 125, OPN, and MK proteins. Mixture of 100 µM hydrogen peroxide in 1 mM hydroquinone was subsequently injected into the system which generated an amperometric signal (Figure 23).

From the obtained signals, it can be noticed that controls exhibited a non-zero signal although controls had no analyte present. This is due to non-specific (NSB) binding of Hrp-MB-Ab2 bioconjugate on the electrode surface although appropriate steps were taken to minimize NSB. Amperometric signal increased as concentrations of the biomarkers increased with all biomarkers exhibiting amperometric signals for concentrations that were 100 times lower than the lowest reported concentration for commercial ELISA. Lower analyte concentrations (0.313 pg/ml – 0.781 pg/ml) generated signals ranging between 7.89 – 9.64 µA/cm^2 than their controls while higher concentrations (31.3 pg/ml – 78.1 pg/ml) generated signals ranging 14.69 - 18.16 µA/cm^2. Although controls generated signals due to NSB, lower concentrations generated signals that are ~ 3.2 times higher than their controls with signals being qualitatively reproducible. Therefore, these results indicate that, multiple biomarkers than be successfully detected using low-cost graphite electrode incorporated into 3D printed fluidic device. It is also capable of detecting analytes concentrations that are 100 times lower than the lower limits of ELISA tests.
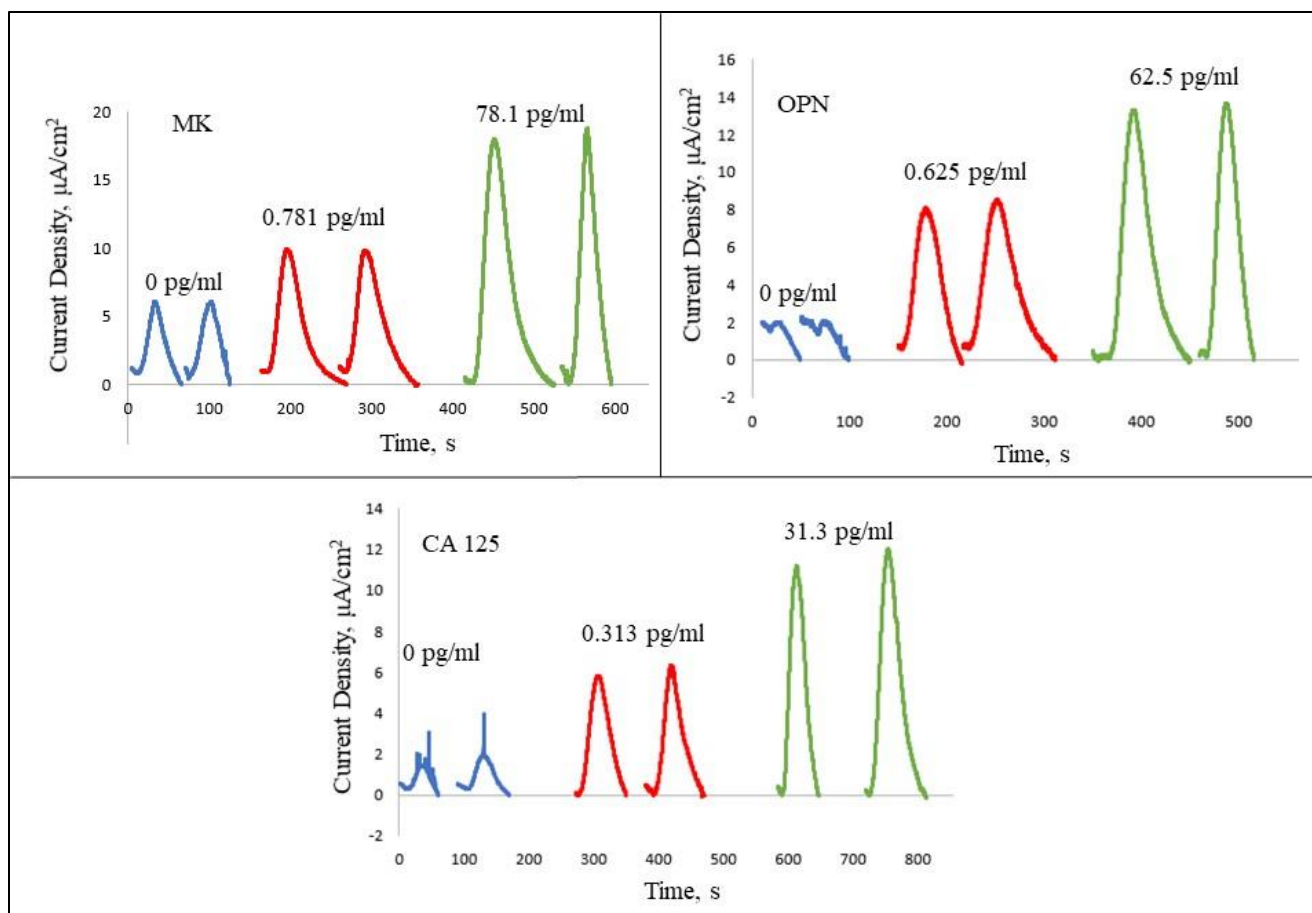
Figure 23. Simultaneous amperometric response for three biomarker detections.A) Response for MK concentrations at 0 pg/ml (control), 0.781 pg/ml (100x lower than LOD of ELISA), 78.1 pg/ml (LOD for ELISA) B) Amperometric signal for OPN concentrations at 0 pg/ml (control), 0.625 pg/ml (100x lower than LOD of ELISA), 62.5 pg/ml (LOD for ELISA) C) Response for CA 125 at concentrations 0 pg/ml (control), 0.313 pg/ml (100x lower than LOD of ELISA), 31.3 pg/ml (LOD for ELISA)

CHAPTER 4. CONCLUSION AND FUTURE WORKS

Advances in research and the use of convenient and effective way to isolate, characterize and detect biomarker proteins has led to a strong emphasis on the development of biomarker panels. However, the most commonly used ELISA technique lacks the ability to detect multiple biomarkers. Sophisticated technologies used in multiple biomarker analysis are rather expensive and often require proprietary reagents. Since multiplex protein biomarker measurements requires large-scale validation studies, there is serious need for simpler, lower cost alternatives. Electrochemical measurements are well-suited for measuring multiple biomarker proteins due to its low-cost, lack of required maintenance, compatibility with multiple measurements and potential for miniaturization.

A combination of electrochemical measurement with 3D printed fluidic device has posed as an alternative platform for multiple biomarkers sensing due to the low cost, ease of operation and fast design to object workflow associated with 3D printing material. In this research, we have exhibited that low cost graphite electrodes modularly incorporated into a 3D printed fluidic device can be used to successfully detect three biomarkers (CA 125, MK, OPN) associated with PSTS electrochemically.

The 3D fluidic device was printed based on dimensions previous report by Bishop et al. and Abdulhamid. Modularly incorporated electrodes were electrochemically characterize using FcMeOH redox probe to ascertain the functionality and reliable of the electrodes for electrochemical measurements which was subsequently modified with AuNP and capture antibodies. By optimizing HRP-MB-Ab2 bioconjugate, and appropriate ratio was used to isolate biomarkers for the sensing strategy. Using an optimized amperometric potential of 0.20 V, a simultaneous electrochemical detection of the three biomarker proteins was achieved with the

antigen-bioconjugate serving as a platform for the electrochemical oxidation and reduction of hydroquinone at a 100 µl/min flow-rate.

While this system has successfully enabled detection of multiple biomarker proteins concentrations that are 100x lower than what is typically analyzed by ELISA, it is important to generate a calibration curve using standard concentrations to determine the sensitivity, limit of detection and dynamic range of the system to which will help measure real human PSTS samples. Although commercially available protein antibodies are proven to be effective in the development of sandwich type assays, some weak binding of analyte and non-target proteins may generate signal, therefore it is important also to evaluate parameters such as cross-reactivity test, spike recovery test in future works.

REFERENCES

1. World Health Organization. Biomarkers & Human Biomonitoring. In *Training for the Health Sector*; 2011; pp 1–35.

2. Strimbu, K.; Tavel, J. A. What Are Biomarkers? *Curr. Opin. HIV AIDS* **2010**, *5* (6), 463–466. https://doi.org/10.1097/COH.0b013e32833ed177.

3. Rusling, J. F. Multiplexed Electrochemical Protein Detection and Translation to Personalized Cancer Diagnostics. *Anal. Chem.* **2013**, *85* (11), 5304–5310. https://doi.org/10.1021/ac401058v.

4. Hooper, C.; Lovestone, S.; Sainz-Fuertes, R. Alzheimer's Disease, Diagnosis and the Need for Biomarkers. *Biomark. Insights* **2008**, *2008* (3), 317–323. https://doi.org/10.4137/BMI.S682.

5. Swift, A.; Heale, R.; Twycross, A. What Are Sensitivity and Specificity? *Evid. Based. Nurs.* **2020**, *23* (1), 2019–2021. https://doi.org/10.1136/ebnurs-2019-103225.

6. Kumar, A.; Gangadharan, B.; Cobbold, J.; Thursz, M.; Zitzmann, N. Absolute quantitation of disease protein biomarkers in a single LC-MS acquisition using apolipoprotein F as an example. Sci. Rep. 2017, 7, 12072.

7. Alabdulwaheed, A. 3D-Printed Fluidic Devices and Incorporated Graphite Electrodes for Electrochemical Immunoassay of Biomarker Proteins. Master's Thesis, East Tennessee State University, Tennessee, U.S.A., **2018**.

8. Aydin, S. A Short History, Principles, and Types of ELISA, and Our Laboratory Experience with Peptide/Protein Analyses Using ELISA. *Peptides* **2015**, *72*, 4–15. https://doi.org/10.1016/j.peptides.2015.04.012

9. Nimse, S. B.; Sonawane, M. D.; Song, K. S.; Kim, T. Biomarker Detection Technologies and Future Directions. *Analyst* **2016**, *141* (3), 740–755. https://doi.org/10.1039/c5an01790d.

10. Xu, Q.; Davis, J. J. The Diagnostic Utility of Electrochemical Impedance. *Electroanalysis* **2014**, *26* (6), 1249–1258. https://doi.org/10.1002/elan.201400035.

11. Sassolas, A.; Blum, L. J.; Leca-Bouvier, B. D. Immobilization Strategies to Develop Enzymatic Biosensors. *Biotechnol. Adv.* **2012**, *30* (3), 489–511. https://doi.org/10.1016/j.biotechadv.2011.09.003.

12. Wu, J.; Fu, Z.; Yan, F.; Ju, H. Biomedical and Clinical Applications of Immunoassays and Immunosensors for Tumor Markers. **2007**, *26* (7), 679–688.

13. Rusling, J. F.; Kumar, C. V.; Gutkind, J. S.; Patel, V. Measurement of Biomarker Proteins for Point-of-Care Early Detection and Monitoring of Cancer. *Analyst* **2010**, *135* (10), 2496–2511. https://doi.org/10.1039/c0an00204f.

14. Danila, D. C.; Pantel, K.; Fleisher, M.; Scher, H. I. Circulating Tumors Cells as Biomarkers: Progress toward Biomarker Qualification. *Cancer J.* **2011**, *17* (6), 438–450. https://doi.org/10.1097/PPO.0b013e31823e69ac.

15. Conway, S. R.; Wong, H. R. Biomarker Panels in Critical Care. *Crit. Care Clin.* **2020**, *36* (1), 89–104. https://doi.org/10.1016/j.ccc.2019.08.007.

16. Cohen, L.; Hartman, M. R.; Amardey-Wellington, A.; Walt, D. R. Digital Direct Detection of MicroRNAs Using Single Molecule Arrays. *Nucleic Acids Res.* **2017**, *45* (14), e137. https://doi.org/10.1093/nar/gkx542.

17. Wu, D.; Milutinovic, M. D.; Walt, D. R. Single Molecule Array (Simoa) Assay with Optimal Antibody Pairs for Cytokine Detection in Human Serum Samples. *Analyst* **2015**, *140* (18), 6277–6282. https://doi.org/10.1039/c5an01238d.

18. Burcu Bahadir, E.; Kemal Sezgintürk, M. Applications of Electrochemical Immunosensors for Early Clinical Diagnostics. *Talanta* **2015**, *132*, 162–174. https://doi.org/10.1016/j.talanta.2014.08.063.

19. Ronkainen, N. J.; Halsall, H. B.; Heineman, W. R. Electrochemical Biosensors. *Chem. Soc. Rev.* **2010**, *39* (5), 1747–1763. https://doi.org/10.1039/b714449k.

20. Heineman, W. R.; Halsall, H. B. Strategies for Electrochemical Immunoassay. *Anal. Chem.* **1985**, *57* (12), 1321–1331. https://doi.org/10.1021/ac00289a804.

21. Choi, J.-W.; Oh, K.; Han, A.; Wijayawardhana, C.; Lannes, C.; Bhansali, S.; Schlueter, K.; Heineman, W.; Halsall, H.; Nevin, J.; Helmicki, A.; Henderson, H.; Ahn, C. Development and Characterization of Microfluidic Devices and Systems for Magnetic Bead-Based Biochemical Detection. *Biomed. Microdevices* **2001**, *3*, 191–200. https://doi.org/10.1023/A:1011490627871.

22. Fowler, J. M.; Wong, D. K. Y.; Brian Halsall, H.; Heineman, W. R. Recent Developments in Electrochemical Immunoassays and Immunosensors. *Electrochem. Sensors, Biosens. their Biomed. Appl.* **2008**, 115–143. https://doi.org/10.1016/B978-012373738-0.50007-6.

23. Arya, S. K.; Estrela, P. Recent Advances in Enhancement Strategies for Electrochemical ELISA-Based Immunoassays for Cancer Biomarker Detection. *Sensors (Switzerland)* **2018**, *18* (7). https://doi.org/10.3390/s18072010.

24. Anik, Ü.; Timur, S. Towards the Electrochemical Diagnosis of Cancer: Nanomaterial-Based Immunosensors and Cytosensors. *RSC Adv.* **2016**, *6* (113), 111831–111841. https://doi.org/10.1039/C6RA23686C.

25. Wei, F.; Patel, P.; Liao, W.; Chaudhry, K.; Zhang, L.; Arellano-Garcia, M.; Hu, S.; Elashoff, D.; Zhou, H.; Shukla, S.; Shah, F.; Ho, C. M.; Wong, D. T. Electrochemical Sensor for Multiplex Biomarkers Detection. *Clin. Cancer Res.* **2009**, *15* (13), 4446–4452. https://doi.org/10.1158/1078-0432.CCR-09-0050.

26. Malhotra, R.; Patel, V.; Vaqué, J. P.; Gutkind, J. S.; Rusling, J. F. Ultrasensitive Electrochemical Immunosensor for Oral Cancer Biomarker IL-6 Using Carbon Nanotube Forest Electrodes and Multilabel Amplification. *Anal. Chem.* **2010**, *82* (8), 3118–3123. https://doi.org/10.1021/ac902802b.

27. Sarkar, P.; Ghosh, D.; Bhattacharyay, D.; Setford, S. J.; Turner, A. P. F. Electrochemical Immunoassay for Free Prostate Specific Antigen (f-PSA) Using Magnetic Beads. *Electroanalysis* **2008**, *20* (13), 1414–1420. https://doi.org/10.1002/elan.200804194.

28. Zani, A.; Laschi, S.; Mascini, M.; Marrazza, G. A New Electrochemical Multiplexed Assay for PSA Cancer Marker Detection. *Electroanalysis* **2011**, *23* (1), 91–99. https://doi.org/10.1002/elan.201000486.

29. Tang, D.; Yuan, R.; Chai, Y. Ultrasensitive Electrochemical Immunosensor for Clinical Immunoassay Using Thionine-Doped Magnetic Gold Nanospheres as Labels and Horseradish Peroxidase as Enhancer. *Anal. Chem.* **2008**, *80* (5), 1582–1588. https://doi.org/10.1021/ac702217m.

30. Che, X.; Yuan, R.; Chai, Y.; Li, J.; Song, Z.; Wang, J. Amperometric Immunosensor for the Determination of α-1-Fetoprotein Based on Multiwalled Carbon Nanotube-Silver Nanoparticle Composite. *J. Colloid Interface Sci.* **2010**, *345* (2), 174–180. https://doi.org/10.1016/j.jcis.2010.01.033.

31. Guo, H.; He, N.; Ge, S.; Yang, D.; Zhang, J. MCM-41 Mesoporous Material Modified Carbon Paste Electrode for the Determination of Cardiac Troponin i by Anodic Stripping Voltammetry. *Talanta* **2005**, *68* (1), 61–66. https://doi.org/10.1016/j.talanta.2005.04.067.

32. Chikkaveeraiah, B. V.; Mani, V.; Patel, V.; Gutkind, J. S.; Rusling, J. F. Microfluidic Electrochemical Immunoarray for Ultrasensitive Detection of Two Cancer Biomarker Proteins in Serum. *Biosens. Bioelectron.* **2011**, *26* (11), 4477–4483. https://doi.org/10.1016/j.bios.2011.05.005.

33. Rusling, J. F.; Bishop, G. W.; Doan, N. M.; Papadimitrakopoulos, F. Nanomaterials and Biomaterials in Electrochemical Arrays for Protein Detection. *J. Mater. Chem. B* **2014**, *2* (1), 12–30. https://doi.org/10.1039/c3tb21323d.

34. Munge, B. S.; Stracensky, T.; Gamez, K.; DiBiase, D.; Rusling, J. F. Multiplex Immunosensor Arrays for Electrochemical Detection of Cancer Biomarker Proteins. *Electroanalysis* **2016**, *28* (11), 2644–2658. https://doi.org/10.1002/elan.201600183.

35. Malhotra, R.; Patel, V.; Chikkaveeraiah, B. V.; Munge, B. S.; Cheong, S. C.; Zain, R. B.; Abraham, M. T.; Dey, D. K.; Gutkind, J. S.; Rusling, J. F. Ultrasensitive Detection of Cancer Biomarkers in the Clinic by Use of a Nanostructured Microfluidic Array. *Anal. Chem.* **2012**, *84* (14), 6249–6255. https://doi.org/10.1021/ac301392g.

36. Krause, C. E.; Otieno, B. A.; Bishop, G. W.; Phadke, G.; Choquette, L.; Lalla, R. V; Peterson, D. E.; Rusling, J. F. Ultrasensitive Microfluidic Array for Serum Pro-Inflammatory Cytokines and C-Reactive Protein to Assess Oral Mucositis Risk in Cancer Patients. *Anal. Bioanal. Chem.* **2015**, *407* (23), 7239–7243. https://doi.org/10.1007/s00216-015-8873-1.

37. Dhanapala, L.; Jones, A. L.; Czarnecki, P.; Rusling, J. F. Sub-Zeptomole Detection of Biomarker Proteins Using a Microfluidic Immunoarray with Nanostructured Sensors. Anal. Chem. 2020, 92 (12), 8021–8025. https://doi.org/10.1021/acs.analchem.0c01507.

38. Chan, H. N.; Tan, M. J. A.; Wu, H. Point-of-Care Testing: Applications of 3D Printing. *Lab Chip* **2017**, *17* (16), 2713–2739. https://doi.org/10.1039/c7lc00397h.

39. Gong, H.; Beauchamp, M.; Perry, S.; Woolley, A. T.; Nordin, G. P. Optical Approach to Resin Formulation for 3D Printed Microfluidics. *RSC Adv.* **2015**, *5* (129), 106621–106632. https://doi.org/10.1039/c5ra23855b.

40. Waheed, S.; Cabot, J. M.; Macdonald, N. P.; Lewis, T.; Guijt, R. M.; Paull, B.; Breadmore, M. C. 3D Printed Microfluidic Devices: Enablers and Barriers. *Lab Chip* **2016**, *16* (11), 1993–2013. https://doi.org/10.1039/c6lc00284f.

41. Beauchamp, M. J.; Nordin, G. P.; Woolley, A. T. Moving from Millifluidic to Truly Microfluidic Sub-100-Mm Cross-Section 3D Printed Devices. *Anal. Bioanal. Chem.* **2017**, *409* (18), 4311–4319. https://doi.org/10.1007/s00216-017-0398-3.

42. Nielsen, A. V; Beauchamp, M. J.; Nordin, G. P.; Woolley, A. T. 3D Printed Microfluidics. *Annu. Rev. Anal. Chem.* **2020**, *13* (1), 45–65. https://doi.org/10.1146/annurev-anchem-091619-102649.

43. Loessberg-Zahl, J.; Van der Meer, A. D.; Van Den Berg, A.; Eijkel, J. C. T. Flow Focusing through Gels as a Tool to Generate 3D Concentration Profiles in Hydrogel-Filled Microfluidic Chips. *Lab Chip* **2019**, *19* (2), 206–213. https://doi.org/10.1039/C8LC01140K.

44. Dixit, C. K.; Kaushik, A. *Microfluidics for Biologists: Fundamentals and Applications*; Springer International Publishing 2016. https://doi.org/10.1007/978-3-319-40036-5.

45. Chan, H. N.; Shu, Y.; Xiong, B.; Chen, Y.; Chen, Y.; Tian, Q.; Michael, S. A.; Shen, B.; Wu, H. Simple, Cost-Effective 3D Printed Microfluidic Components for Disposable, Point-of-Care Colorimetric Analysis. *ACS Sensors* **2016**, *1* (3), 227–234. https://doi.org/10.1021/acssensors.5b00100.

46. Bishop, G. W.; Satterwhite-Warden, J. E.; Bist, I.; Chen, E.; Rusling, J. F. Electrochemiluminescence at Bare and DNA-Coated Graphite Electrodes in 3D-Printed Fluidic Devices. *ACS Sensors* **2016**, *1* (2), 197–202. https://doi.org/10.1021/acssensors.5b00156.

47. Erkal, J. L.; Selimovic, A.; Gross, B. C.; Lockwood, S. Y.; Walton, E. L.; McNamara, S.; Martin, R. S.; Spence, D. M. 3D Printed Microfluidic Devices with Integrated Versatile and Reusable Electrodes. *Lab Chip* **2014**, *14* (12), 2023–2032. https://doi.org/10.1039/c4lc00171k.

48. Shahrubudin, N.; Lee, T. C.; Ramlan, R. An Overview on 3D Printing Technology: Technological, Materials, and Applications. *Procedia Manuf.* **2019**, *35*, 1286–1296. https://doi.org/10.1016/j.promfg.2019.06.089.

49. Rajkumari, K.; Chandra, P.; Balaji, P. Three-Dimensional Printing-a Revolutionary Technology. *J. Clin. Diagnostic Res.* **2018**, *12* (12), 12–18. https://doi.org/10.7860/JCDR/2018/37752.12410.

50. Zhou, H.; Bhaduri, S. B. *3D Printing in the Research and Development of Medical Devices*; Elsevier Inc., 2018. https://doi.org/10.1016/B978-0-12-813477-1.00012-8.

51. ASTM F2792-12a, Standard terminology for additive manufacturing technologies. ASTM International. West Conshohocken, PA, 2012.

52. Bhargava, K. C.; Thompson, B.; Malmstadt, N. Discrete Elements for 3D Microfluidics. *Proc. Natl. Acad. Sci. U. S. A.* **2014**, *111* (42), 15013–15018. https://doi.org/10.1073/pnas.1414764111.

53. Shallan, A. I.; Smejkal, P.; Corban, M.; Guijt, R. M.; Breadmore, M. C. Cost-Effective Three-Dimensional Printing of Visibly Transparent Microchips within Minutes. *Anal. Chem.* **2014**, *86* (6), 3124–3130. https://doi.org/10.1021/ac4041857.

54. Sun, C.; Fang, N.; Wu, D. M.; Zhang, X. Projection Micro-Stereolithography Using Digital Micro-Mirror Dynamic Mask. *Sensors Actuators, A Phys.* **2005**, *121* (1), 113–120. https://doi.org/10.1016/j.sna.2004.12.011.

55. Bhattacharjee, N.; Urrios, A.; Kang, S.; Folch, A. The Upcoming 3D-Printing Revolution in Microfluidics. *Lab Chip* **2016**, *16* (10), 1720–1742. https://doi.org/10.1039/c6lc00163g.

56. Ngo, T. D.; Kashani, A.; Imbalzano, G.; Nguyen, K. T. Q.; Hui, D. Additive Manufacturing (3D Printing): A Review of Materials, Methods, Applications and Challenges. *Compos.*

Part B Eng. **2018**, *143* (December 2017), 172–196.
https://doi.org/10.1016/j.compositesb.2018.02.012.

57. Rogers, C. I.; Qaderi, K.; Woolley, A. T.; Nordin, G. P. 3D Printed Microfluidic Devices
with Integrated Valves. *Biomicrofluidics* **2015**, *9* (1). https://doi.org/10.1063/1.4905840.

58. Castiaux, A. D.; Currens, E. R.; Martin, R. S. Direct Embedding and Versatile Placement of
Electrodes in 3D Printed Microfluidic-Devices. *Analyst* **2020**, *145* (9), 3274–3282.
https://doi.org/10.1039/d0an00240b.

59. Cardoso, R. M.; Kalinke, C.; Rocha, R. G.; dos Santos, P. L.; Rocha, D. P.; Oliveira, P. R.;
Janegitz, B. C.; Bonacin, J. A.; Richter, E. M.; Munoz, R. A. A. Additive-Manufactured
(3D-Printed) Electrochemical Sensors: A Critical Review. *Anal. Chim. Acta* **2020**, *1118*,
73–91. https://doi.org/10.1016/j.aca.2020.03.028.

60. O'Neil, G. D.; Ahmed, S.; Halloran, K.; Janusz, J. N.; Rodríguez, A.; Terrero Rodríguez, I.
M. Single-Step Fabrication of Electrochemical Flow Cells Utilizing Multi-Material 3D
Printing. *Electrochem. commun.* **2019**, *99* (December 2018), 56–60.
https://doi.org/10.1016/j.elecom.2018.12.006.

61. Kadimisetty, K.; Mosa, I. M.; Malla, S.; Satterwhite-Warden, J. E.; Kuhns, T. M.; Faria, R.
C.; Lee, N. H.; Rusling, J. F. 3D-Printed Supercapacitor-Powered
Electrochemiluminescent Protein Immunoarray. *Biosens. Bioelectron.* **2016**, *77*, 188–
193. https://doi.org/10.1016/j.bios.2015.09.017.

62. Kadimisetty, K.; Malla, S.; Bhalerao, K. S.; Mosa, I. M.; Bhakta, S.; Lee, N. H.; Rusling, J.
F. Automated 3D-Printed Microfluidic Array for Rapid Nanomaterial-Enhanced
Detection of Multiple Proteins. *Anal. Chem.* **2018**, *90* (12), 7569–7577.
https://doi.org/10.1021/acs.analchem.8b01198.

63. National Cancer Institute Homepage. https://www.cancer.gov/types/soft-tissue-
sarcoma/hp/child-soft-tissue-treatment/ (accessed 2021-14-17)

64. Thompson, P. A.; Chintagumpala, M. Targeted Therapy in Bone and Soft Tissue Sarcoma in
Children and Adolescents. *Curr. Oncol. Rep.* **2012**, *14* (2), 197–205.
https://doi.org/10.1007/s11912-012-0223-2.

65. Sandoval, J. A.; Malkas, L. H.; Hickey, R. J. Clinical Significance of Serum Biomarkers in
Pediatric Solid Mediastinal and Abdominal Tumors. *Int. J. Mol. Sci.* **2012**, *13* (1), 1126–
1153. https://doi.org/10.3390/ijms13011126.

66. Lucas, S.; Reindl, T.; Henze, G.; Kurtz, A.; Sakuma, S.; Driever, P. H. Increased Midkine
Serum Levels in Pediatric Embryonal Tumor Patients. *J. Pediatr. Hematol. Oncol.* **2009**,
31 (10), 713–717. https://doi.org/10.1097/MPH.0b013e3181b6db9f.

67. Bache, M.; Kappler, M.; Wichmann, H.; Rot, S.; Hahnel, A.; Greither, T.; Said, H. M.; Kotzsch, M.; Würl, P.; Taubert, H.; Vordermark, D. Elevated Tumor and Serum Levels of the Hypoxia-Associated Protein Osteopontin Are Associated with Prognosis for Soft Tissue Sarcoma Patients. *BMC Cancer* **2010**, *10*. https://doi.org/10.1186/1471-2407-10-132.

68. Bishop, G. W.; Satterwhite-Warden, J. E.; Bist, I.; Chen, E.; Rusling, J. F. Electrochemiluminescence at Bare and DNA-Coated Graphite Electrodes in 3D-Printed Fluidic Devices. ACS. Sens. 2016, 1, 197–202.

69. TechNotes | Bangs Laboratories, Inc. https://www.bangslabs.com/support/technical support/technotes (accessed May 25, 2021)

70. Navratil, R.; Kotzianova, A.; Halouzka, V.; Opletal, T.; Triskova, I.; Trnkova, L.; Hrbac, J. Polymer Lead Pencil Graphite as Electrode Material: Voltammetric, XPS and Raman Study. *J. Electroanal. Chem.* **2016**, *783*, 152–160. https://doi.org/10.1016/j.jelechem.2016.11.030.

71. Kariuki, J. K. An Electrochemical and Spectroscopic Characterization of Pencil Graphite Electrodes. *J. Electrochem. Soc.* **2012**, *159* (9), H747–H751. https://doi.org/10.1149/2.007209jes.

72. Tasić, Ž. Z.; Petrović Mihajlović, M. B.; Simonović, A. T.; Radovanović, M. B.; Antonijević, M. M. Review of Applied Surface Modifications of Pencil Graphite Electrodes for Paracetamol Sensing. *Results Phys.* **2021**, *22* (January). https://doi.org/10.1016/j.rinp.2021.103911.

73. Nery, E. W.; Kundys-Siedlecka, M.; Furuya, Y.; Jönsson-Niedziółka, M. Pencil Lead as a Material for Microfluidic 3D-Electrode Assemblies. *Sensors (Switzerland)* **2018**, *18* (11). https://doi.org/10.3390/s18114037.

74 Aoki, K.; Okamoto, T.; Kaneko, H.; Nozaki, K.; Negishi, A. Applicability of Graphite Reinforcement Carbon Used as the Lead of a Mechanical Pencil to Voltammetric Electrodes. *J. Electroanal. Chem.* **1989**, *263* (2), 323–331. https://doi.org/10.1016/0022-0728(89)85102-2

75. Tavares, P. H. C. P.; Barbeira, P. J. S. Influence of Pencil Lead Hardness on Voltammetric Response of Graphite Reinforcement Carbon Electrodes. *J. Appl. Electrochem.* **2008**, *38* (6), 827–832. https://doi.org/10.1007/s10800-008-9518-2.

76. Ogbu, C.I.; Feng, X.; Dada, S.N.; Bishop, G.W. Screen-Printed Soft-Nitrided Carbon Electrodes for Detection of Hydrogen Peroxide. *Sensors* **2019**, *19*, 3741. https://doi.org/10.3390/s19173741

77. Bishop, G. W., Ahiadu, B. K., Smith, J. L., & Patterson, J. D. (2017). Use of Redox Probes for Characterization of Layer-by-Layer Gold Nanoparticle-Modified Screen-Printed

Carbon Electrodes. *Journal of The Electrochemical Society*, *164*(2), B23–B28. https://doi.org/10.1149/2.0431702jes

78. Gowda, J. I.; Nandibewoor, S. T. Electrochemical Characterization and Determination of Paclitaxel Drug Using Graphite Pencil Electrode. *Electrochim. Acta* **2014**, *116*, 326–333. https://doi.org/10.1016/j.electacta.2013.11.014.

79. David, I. G.; Popa, D.-E.; Buleandra, M. Pencil Graphite Electrodes: A Versatile Tool in Electroanalysis. *J. Anal. Methods Chem.* **2017**, *2017*, 1905968. https://doi.org/10.1155/2017/1905968.

80. Haiss, W.; Thanh, N. T. K.; Aveyard, J.; Fernig, D. G. Determination of Size and Concentration of Gold Nanoparticles from UV−Vis Spectra. *Anal. Chem.* **2007**, *79* (11), 4215–4221. https://doi.org/10.1021/ac0702084.

81. Mani, V.; Chikkaveeraiah, B. V.; Patel, V.; Gutkind, J. S.; Rusling, J. F. Ultrasensitive Immunosensor for Cancer Biomarker Proteins Using Gold Nanoparticle Film Electrodes and Multienzyme-Particle Amplification. ACS. Nano. 2009, 3 (3), 585–594

82. Mani, V.; Wasalathanthri, D. P.; Joshi, A. A.; Kumar, C. V.; Rusling, J. F. Highly Efficient Binding of Paramagnetic Beads Bioconjugated with 100,000 or More Antibodies to Protein-Coated Surfaces. Anal. Chem. 2012, 84, 10485–10491.

83. Andreasson, U.; Perret-Liaudet, A.; van Waalwijk van Doorn, L. J. C.; Blennow, K.; Chiasserini, D.; Engelborghs, S.; Fladby, T.; Genc, S.; Kruse, N.; Kuiperij, H. B.; Kulic, L.; Lewczuk, P.; Mollenhauer, B.; Mroczko, B.; Parnetti, L.; Vanmechelen, E.; Verbeek, M. M.; Winblad, B.; Zetterberg, H.; Koel-Simmelink, M.; Teunissen, C. E. A Practical Guide to Immunoassay Method Validation. *Front. Neurol.* **2015**, *6* (Aug), 1–8. https://doi.org/10.3389/fneur.2015.00179.

VITA

IVY ANTWI

Education:	M.S. Chemistry, East Tennessee State University, Johnson City, Tennessee, 2021
	B.Sc. Chemistry, Kwame Nkrumah University of Science and Technology, Kumasi, Ghana, 2017
Professional Experience:	Analyst, Ghana Standards Authority; Accra, Ghana, 2017-2019
	Graduate Assistant, East Tennessee State University, College of Arts and Sciences, 2019-2021
Honors and Awards:	First Class Honors, KNUST, 2017